

MiXDM: Cosmic Ray Signals from Multiple States of Dark Matter

Ilias Cholis and Neal Weiner

*Center for Cosmology and Particle Physics, Dept. of Physics, New York University,
New York, NY 10003*

E-mail: nw32@nyu.edu, ijc219@nyu.edu

ABSTRACT: Recent data from cosmic ray experiments such as PAMELA, Fermi, ATIC and PPB-BETS all suggest the need for a new primary source of electrons and positrons at high ($\gtrsim 100$ GeV) energies. Many proposals have been put forth to explain these data, usually relying on a single particle to annihilate or decay to produce e^\pm . In this paper, we consider models with multiple species of WIMPs with significantly different masses. We show if such dark matter candidates χ_i annihilate into light bosons, they naturally produce equal annihilation rates, even as the available numbers of pairs for annihilation $n_{\chi_i}^2$ differ by orders of magnitude. We argue that a consequence of these models can be to add additional signal naturally at lower (~ 100 GeV) versus higher (\sim TeV) energies, changing the expected spectrum and even adding bumps at lower energies, which may alleviate some of the tension in the required annihilation rates between PAMELA and Fermi. These spectral changes may yield observable consequences in the microwave Haze signal observed at the upcoming Planck satellite. Such a model can connect to other observable signals such as DAMA and INTEGRAL by having the lighter (heavier) state be a pseudo-Dirac fermion with splitting 100 keV (1 MeV). We show that variations in the halo velocity dispersion can alleviate constraints from final state radiation in the galactic center and galactic ridge. If the lighter WIMP has a large self-interaction cross section, the light-WIMP halo might collapse, dramatically altering expectations for direct and indirect detection signatures.

KEYWORDS: Dark Matter, Planck, PAMELA.

Contents

1. Introduction	1
2. Dark Matter with Multiple Components	2
2.1 Annihilation rates	3
3. Models of MiXDM	4
4. Electron and Positron Signals of Multiple WIMPs	6
4.1 Annihilations with Different Force Carriers	7
4.2 Inverse Compton Signals at Fermi	8
4.3 General fits and constraints	9
5. Counting the number of WIMP species with Synchrotron radiation	12
5.1 Modeling Synchrotron Emission with Power Laws	12
5.2 Dependence of the B-field vs ISRF assumptions	18
6. 3 masses	19
7. Scattering and Effects on the DM Halo	20
8. Conclusions	21
A. DM Halo and CR propagation	22
B. Review of Synchrotron Emission	23

1. Introduction

Signals from a wide range of sources have prompted a rethinking of the nature of dark matter. The positron fraction of cosmic rays has shown a steep rise [1], implying the presence of a new primary source of antimatter. The Fermi [2], ATIC [3] and PPB-BETS [4] experiments all show a harder spectrum of e^\pm at high ($\gtrsim 100$ GeV) energies than had been predicted from secondary production, with a break at ~ 1 TeV seen at Fermi and HESS [5] [6]. Data from INTEGRAL suggest a new source of low energy positrons, while the DAMA modulation signal has extended to 8.2σ .

Remarkably, there is a simple “unified” framework that explains all of these anomalies [7]. One of the principle changes is that rather than annihilating to standard model channels, the

WIMP can annihilate dominantly into a new light, unstable boson, which in turn maintains equilibrium with the standard model and decays through a small mixing parameter [8]. The light mass kinematically prevents production of antiprotons [9], allowing consistency with the PAMELA antiproton measurements [10]. Such scenarios have been widely discussed in the context of present dark matter anomalies [8, 11, 9, 7, 12, 13, 14, 15].

In SUSY models, the LSP is stable by R-parity, and thus there is a unique WIMP candidate. In contrast, in these models, the symmetry stabilizing the dark matter against decay is not R-parity, and thus there is no compelling reason that there should be a single stable neutral particle. Indeed, it is very possible - perhaps even likely - that there are a variety of parities in the theory, and that many different particles together comprise the dark matter. We shall see that in models where dark matter freezes out by annihilation into a light boson, the annihilation rates of different components of dark matter *are naturally equal*, even though n_χ^2 can differ between the species by orders of magnitude. As a consequence, the spectra of positrons and electrons can have interesting structures, including crests and troughs. This phenomenon arises naturally, without any tuning of the parameters. Such a model can alleviate some tension between PAMELA, which seems to require somewhat larger cross sections at lower energy, and Fermi, which requires lower cross sections but extending to higher energy.

In such models, one can explain the INTEGRAL signal with a heavy (\sim TeV) mass state exciting into an MeV excited state as in [8], while explaining DAMA through a lighter (\sim 100 GeV) state exciting into a \sim 100 keV excited state, as in [16, 17]. This scenario, to employ multiple states for inelastic and exciting dark matter (which we refer to as MiXDM) was proposed in [18]. Although DAMA and INTEGRAL both play roles in motivating the spectrum considered, we shall not focus on these aspects, focusing instead on the higher energy cosmic ray signals (and their synchrotron counterparts). Because of the motivation in [18], we shall generically refer to these models, in which multiple states annihilate comparably into light bosons, as “MiXDM” models.

In this paper, we shall explore the possibility of testing such a scenario. In section 2, we will review the setup and in section 3 the model building issues, including models where different annihilation channels arise. In section 4, we discuss the cosmic ray signatures from such a scenario, and discuss the interesting spectral features that can arise. In 5, we go beyond the e^+e^- signals, we shall argue that signatures in the microwave haze of the inner galaxy may help to show if the dark sector has multiple components. In section 6 we consider further generalizations, with more states, while in section 7, we note the important changes to direct detection experiments that can arise. Finally, we conclude in section 8.

2. Dark Matter with Multiple Components

The idea that dark matter has multiple components is not new. In [19, 20], it was argued that a subdominant component of dark matter in the halo could still give significant signals at direct detection experiments, and indirect signals related to WIMP capture (such as in the

Earth). [21] argued that a sector combining a TeV WIMP together with a GeV mass WIMP could explain PAMELA and DAMA. As we have already noted, [18] constructed a model in which a TeV particle was responsible for the high energy e^\pm signatures, as well as the 511 keV emission observed by INTEGRAL, while a separate particle with a 100 keV splitting would explain DAMA.

Our effort here is not to focus on the direct detection signals of multiple states, but rather their *indirect* signals. We shall see that if dark matter freezes out and annihilates presently into a light force carrier, the annihilation rates are naturally equal. Because the lighter WIMP has its signal compressed into a narrower energy range, this can lead to an enhancement of e^\pm at lower energies, possibly even yielding a bump in the e^+ or $e^+ + e^-$ spectrum.

2.1 Annihilation rates

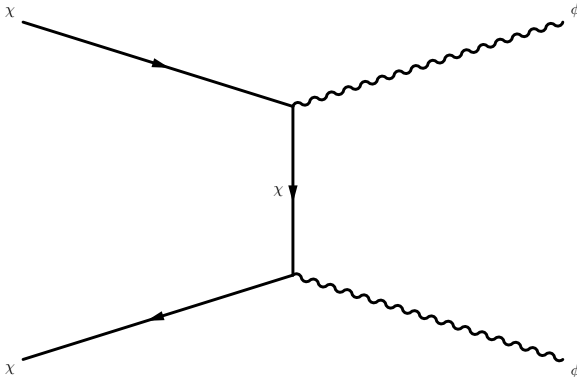


Figure 1: Perturbative annihilation of dark matter into ϕ .

Let us begin by sketching out the process described in [8] whereby dark matter freezes out through annihilations into a new metastable force carrier ϕ , to which it couples with strength g . The annihilation proceeds through the diagram shown in figure 1, and has a cross section (at high energy) that scales as

$$\sigma v \sim \frac{\alpha^2}{M_\chi^2}. \quad (2.1)$$

The dark matter stays in thermal equilibrium with the standard model through the interactions of ϕ with the standard model, in particular the process $e\phi \leftrightarrow e\gamma$ or $\phi\phi \leftrightarrow f\bar{f}$, depending on the model. As was emphasized in [8, 11, 22, 23], this allows the “WIMP miracle” to function, even though the WIMP has no strong interactions to the standard model. Thus, one has the usual relation [24] that the dark matter density scales inversely with cross section. I.e.,

$$\rho \sim \frac{1}{\langle\sigma v\rangle} \sim M_\chi^2, \quad (2.2)$$

where we focus only on the dominant mass scaling. The annihilation rate of the dark matter in the present universe then simply scales as

$$n_\chi^2 \langle \sigma v \rangle \sim \left(\frac{\rho}{M_\chi} \right)^2 \frac{1}{M_\chi^2} \sim \text{constant}. \quad (2.3)$$

Remarkably, because the number density scales as mass, the leading dependencies cancel precisely. Thus one sees immediately that *in scenarios where the dark matter freezes out through annihilations into a light force carrier, the annihilation rates of species of different mass are naturally equal.*¹

There are of course caveats to this. We are assuming that the coupling g is the same between the states. This arises automatically if ϕ is a boson of a new gauge group under which χ_i have the same representation, or if there is a symmetry relating the different χ_i , broken softly by their masses. The Sommerfeld effect [25, 26, 27, 28, 23, 12], which is often invoked to explain the high cross sections needed to explain the cosmic ray data, can for instance have already saturated for one WIMP and not the other, or be in a v^{-2} resonance region for one and not the other. Factors of two can arise as well for fermions versus scalars, or if the representations of the groups are not identical. Finally, there is the usual logarithmic dependence on mass. That said, it is important to note that the *starting point* for consideration is that the annihilation rates should be comparable, and such effects can be invoked to move away from that.

3. Models of MiXDM

Scenarios where multiple states are present are trivial to construct. Probably the easiest means to do this is to WIMPs which are charged under a new $U(1)_{dark}$, with gauge field ϕ_μ , as was first considered by [29]. To this we add a small \lesssim GeV mass to the gauge boson, and a small splitting δ between the Majorana states for the WIMPs.

$$\mathcal{L} = \bar{\chi}_i \not{D} \chi_i + \frac{1}{4} F_{\mu\nu}^d F^{d\mu\nu} + \epsilon F_{\mu\nu} F^{d\mu\nu} + m^2 \phi_\mu \phi^\mu + M_i \bar{\chi}_i \chi_i + \delta_i \chi_i \chi_i. \quad (3.1)$$

One can also trivially replace the fermionic WIMP with a complex scalar.

$$\mathcal{L} = (D_\mu \chi_i)^* D_\mu \chi_i + \frac{1}{4} F_{\mu\nu}^d F^{d\mu\nu} + \epsilon F_{\mu\nu} F^{d\mu\nu} + m^2 \phi_\mu \phi^\mu + M_i^2 \chi_i^* \chi_i + M_i \delta_i \chi_i \chi_i. \quad (3.2)$$

Here i indexes the WIMP species, and we have suppressed the necessary dark Higgs mechanism. Reduced to a single species with $\delta \approx 1\text{MeV}$, this is just the original XDM model proposed by [8]. To explain INTEGRAL, such a model requires a double excitation. If the Milky Way halo has a uniform and low velocity dispersion, it is difficult to achieve this, as pointed

¹Note that while we are focused on models with new force carriers, this would also be true for annihilations into W 's, Z 's, or even light fermions, so long as the WIMP mass were suitably large compared to the particle into which it annihilated.

out by [30], prompting development of single excitation models [8, 7] and inverted models [31, 32], which more easily satisfy the INTEGRAL rate due to the naturally large scattering cross section from the light mediator [8]. Some recent simulations involving baryons show a significant increase of the velocity dispersion in the galactic center [33, 34, 35, 36, 37], which can alleviate these constraints [38, 39], possibly opening the possibility of double-excitations, although this is unclear.

Meanwhile, the interaction with the standard model can allow us to construct models of inelastic dark matter [7]. Since heavier WIMPs have lower modulation fraction, the constraints on them are stronger [17, 40, 41, 42, 43]. While simulations and simulation-inspired halo models allow for heavier WIMPs [40, 44], having two WIMPs is a simple approach to this problem as well. Note that the annihilation cross section goes as α_{dark}^2/M_i^2 while the scattering cross section scales as ϵ^2/m_ϕ^4 . Thus, even a subdominant WIMP can have significant scattering cross sections, even beyond the natural “order one” level considered by [19].

Thus, taking the above Lagrangian with two species one arrives at the MiXDM scenario, which, suitably supersymmetrized, is just the setup proposed by [18].

We note that if there is an approximate symmetry protecting the WIMPs from both M and δ , it is natural that δ_i/M_i is constant, or at least roughly so.

An interesting generalization of this would be to a situation with *two* U(1)’s in the dark sector (or even more generally, each WIMP would have its own U(1)). I.e., we would modify 3.1 by

$$\frac{1}{4}F_{i\mu\nu}^d F_i^{d\mu\nu} + \epsilon F_{\mu\nu} F_i^{d\mu\nu} + m_i^2 \phi_{i\mu} \phi_i^\mu \quad (3.3)$$

In this case, it is reasonable to expect that the soft breaking of the masses for χ would radiatively feed into determining the masses of the ϕ . Thus, one would expect $m_i/M_i = \text{constant}$. This could be generated for instance when the WIMPs, themselves, serve as gauge mediators for the masses of the ϕ ’s as described by [23, 45], but not in cases where the mediation was dominated by the effective D-terms, as in [46, 18, 47].

Finally, we can consider situations where ϕ is a scalar, and there is a Z_2 symmetry between the two WIMPs. I.e., we could consider

$$\mathcal{L} = \bar{\chi}_i \not{\partial} \chi_i + \partial_\mu \phi^* \partial^\mu \phi + \lambda \phi^2 h^\dagger h + m^2 \phi^2 + (g\phi + M_i) \bar{\chi} \chi + \delta_i \chi \chi \quad (3.4)$$

Which can be generalized to a multi- ϕ theory trivially, in which case again, one could argue that the ϕ_i masses would be proportional to the χ_i masses. The scalar mediated theories can yield XDM phenomenology, but is difficult to produce the iDM phenomenology naturally [48]. Since our focus is on cosmic rays, the particular Lorentz representation is not especially crucial, but a scenario with the DAMA signal likely fits best with vectors.

We should note that there are a wide variety of studies on the possibility of light force carriers. [49] first studied them in the context of MeV scale dark matter, as an explanation of INTEGRAL. While XDM is limited to $\sim \text{TeV}$ masses for χ and $100 \text{ MeV} \sim \text{GeV}$ for ϕ , [11] considered the setup for a much wider kinematical range, including MeV WIMPs and

~ 20 GeV force carriers. Decaying models have also invoked new light force carriers [50, 51] While we focus on cosmic ray signals here, a broad set of collider and other accelerator studies [52, 46, 53, 54, 55, 56, 57] as well as astrophysical signatures [58, 59, 60, 61, 62, 63] will be essential in testing this picture. (For a broad review of existing and future limits, see [60].)

4. Electron and Positron Signals of Multiple WIMPs

Before progressing to consider in details the electron signals from multiple WIMPs, we can sketch out what sort of range of signals is possible. The simplest scenario is to consider two WIMPs, of mass $M_1 \sim 100$ GeV and $M_2 \sim 1$ TeV, annihilating through the channel $\chi\chi \rightarrow \phi\phi$ with $\phi \rightarrow e^+e^-$ (which naturally occurs for $m_\phi < 2m_\mu$). We calculate the cosmic ray spectra as described in appendix A, and show the results in figure 2. Here we see immediately the important consequence of this scenario. Although the standard case of a heavy WIMP annihilating through this channel yields very hard spectra, the inclusion of the lighter WIMP leads to a softening. Indeed, with a slightly higher rate than equal (which can arise, as described, from scalar/fermion differences, or differences in the Sommerfeld effect), bump like features can appear in the spectrum. This is possibly the most important point of this section: *the presence of bumps or a flattening in the positron spectrum may indicate the presence of a second, lighter WIMP*. Although no such features have been found at this point, future data releases may show them as PAMELA goes to higher energies and with the higher statistics and energies of AMS-02 [64].²

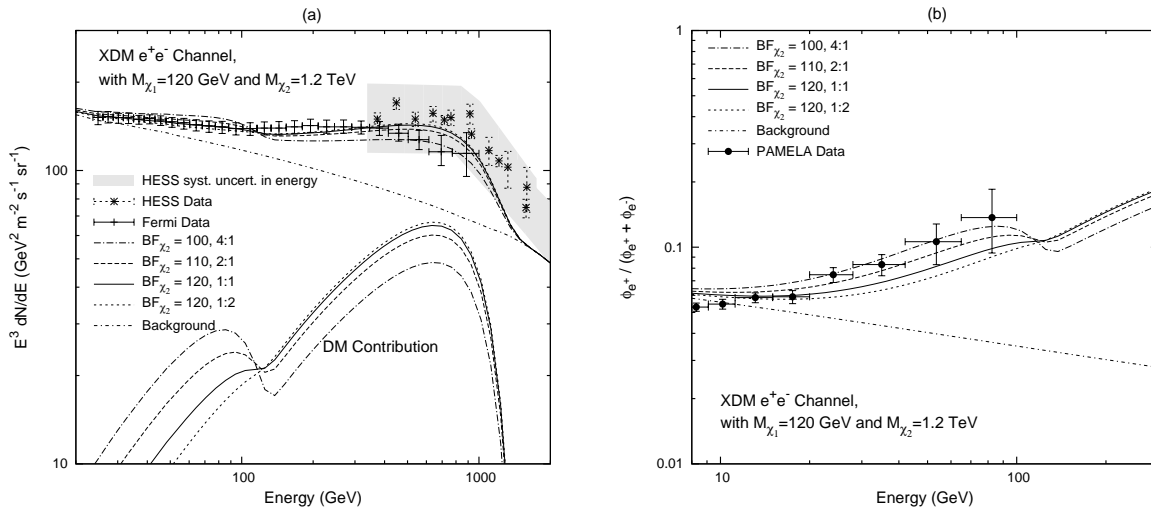


Figure 2: Fermi/HESS electron plus positron (*left*) and PAMELA positron (*right*) signals from annihilation of 2 XDM species with $M_{\chi_1} = 120$ GeV and $M_{\chi_2} = 1.2$ TeV through e^\pm channel. BF specifies the cross section of the heavier WIMP while $x : y$ specifies the lighter WIMP has an annihilation rate x/y times that of the heavier.

²Note that the parameters chosen here, as in the examples through this paper, are consistent with the CMB limits described in [65, 66, 67].

Such “bumpy” features have been considered before in the context of pulsars [68, 69, 70], where bumps are associated with the duration between the initial release of positrons from the pulsar wind nebula and the present time. Although it is likely difficult to get some of the truly “spikey” signals considered by [68, 69, 70], it is intriguing that broader features can be realized quite naturally for annihilating WIMP models, and are even expected in theories with multiple WIMPs (see additionally [71] for a discussion of such features from multi-WIMP setups in decaying models) as well as pulsars.

While in figure 2 we have varied the relative annihilation rates slightly, we can also vary the mass of the lighter state, which we do in figure 3. In cases where the lighter WIMP has a slightly larger cross section (plotted 2:1) the “feature” produced in the e^\pm spectrum would seem in tension with the Fermi data if it is too high ($\gtrsim 150$ GeV). Lighter WIMPs seem to have a good fit with the Fermi data, and it is intriguing to speculate on the change in slope in the experiment Fermi electron data. This slope change, while not statistically significant, could arise from the break associated with a ~ 100 GeV WIMP into light force carriers. Should this persist in the future, it may be pointing to the MiXDM scenario.

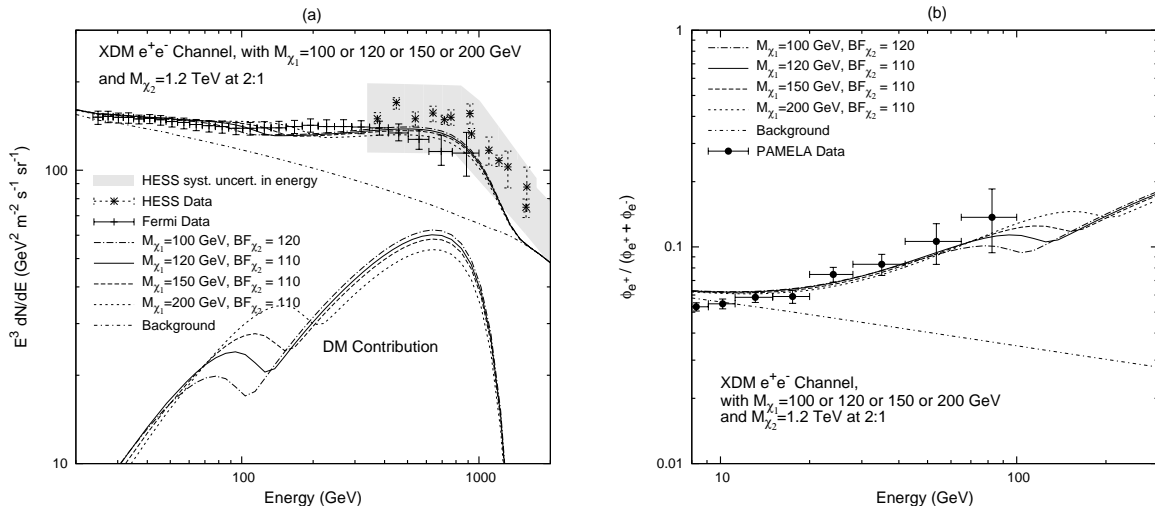


Figure 3: Cosmic ray signals as in Fig. 2, with $M_{\chi_1} = 100, 120, 150, 200$ GeV and $M_{\chi_2} = 1.2$ TeV through the XDM e^\pm channel.

4.1 Annihilations with Different Force Carriers

As noted above, it is possible to have different WIMPs, each with its own ϕ_i . It is natural to expect in this case that the ϕ_i would receive different radiative corrections to their masses, which could naturally yield a situation where $M_i : \delta_i : m_i$ was constant.

As a means to study this, we will consider the situation where the lighter particle annihilates as $2\chi_1 \rightarrow 2\phi_1$ and then the mediator decays to leptons $\phi_1 \rightarrow l^+l^-$, while the heavier annihilates to $2\chi_2 \rightarrow 2\phi_2$ where $\phi_2 \rightarrow 2\phi_2'$ that ϕ_2' then decays to l^+l^- . For the analytical formulas for the injection spectra of the e^\pm one can see [72, 73].

In Fig. 4 we show the results where $l = e$ or $l = \mu$. This results in a very smooth change of the $e^+ + e^-$ flux at $E = M_{\chi_1}$ relative to that of just χ_2 , for cases where relative annihilation rates of 1:1 are assumed. Both cases provide good fit to the Fermi data while their projected (B.F. calculated from fitting only to the Fermi data) positron fraction agrees with the PAMELA data.

In Fig. 4a,b we show the case where $M_{\chi_1} = 200\text{GeV}$ annihilating to $2\phi_1$ with $m_{\phi_1} < 2m_\mu$, thus $\phi_1 \rightarrow e^+e^-$ (XDM e^+e^- channel) and $M_{\chi_2} = 1.6\text{TeV}$ annihilating to $2\phi_2$ where $\phi_2 \rightarrow 2\phi'_2$ with $m_{\phi_2} \simeq 10m_{\phi'_2}$ and $\phi'_2 \rightarrow e^+e^-$ as $m_{\phi'_2} < 2m_\mu$ (XDM 2-step e^+e^- channel). In Fig. 4c,d we study the case where $M_{\chi_1} = 300\text{GeV}$ and $M_{\chi_2} = 3.6\text{TeV}$ with $2m_\mu < m_{\phi_1}, m_{\phi'_2} < 2m_\pi$, thus the final product of the annihilations of the two species are $\mu^+\mu^-$ ($\phi_1, \phi'_2 \rightarrow \mu^+\mu^-$), (XDM $\mu^+\mu^-$ channel for the lighter and XDM 2-step $\mu^+\mu^-$ channel for the heavier species). Finally in Fig. 4e,f we study the case where $M_{\chi_1} = 250\text{GeV}$ annihilating through XDM e^+e^- channel and $M_{\chi_2} = 2.7\text{TeV}$ through XDM $\mu^+\mu^-$ channel. Our choices for M_{χ_2} are suggested by the need to fit to the Fermi data and not violate the HESS upper limits on the e^+e^- flux. As 2-body cascade decays of ϕ 's and 3-body decays of muons produce significantly softer injection spectra of e^\pm than XDM e^+e^- , higher masses of M_{χ_2} are needed to fit to the Fermi data.

In viewing the various examples of MiXDM annihilation signals, there are a few important issues that present themselves: first, while 4:1 rates typically clearly exhibit a feature in the electron and/or positron spectra, they are also generally in strong tension with the current Fermi data as well. Signals with 2:1 and smaller ratios are more difficult to distinguish in the electronic spectra. At the same time, the projected positron fraction fits the PAMELA data well for ratios of 1:1 and 2:1, alleviating some existing tension between the suggested annihilation rates from Fermi vs PAMELA data in single WIMP scenarios. Finally, should such a signal be present in the upcoming experimental results, it will still be unclear whether this is arising from dark matter, or from a conventional astrophysical source, such as pulsars. To answer the question whether a second WIMP is present in the data, we seek an additional means to constrain the signal.

4.2 Inverse Compton Signals at Fermi

As has been discussed elsewhere [74, 75, 76, 77, 78, 79, 80], models of WIMPs that explain PAMELA/Fermi also yield a substantial gamma ray signal in the galactic center region from inverse-Compton scattering. Remarkably, based upon the Fermi data release [81] have argued that such a signal is present. Because MiXDM models have an additional soft e^\pm component, this can modify the spectrum of gamma rays.

We show an example of the gamma ray spectrum for a MiXDM model in Fig 5. A somewhat smaller boost in the Haze region seems to give an additional contribution to the gamma rays which is at high energies comparable to what is extracted in [81]. Such a variation could be easily accounted for by a v^{-1} scaling, as shown.

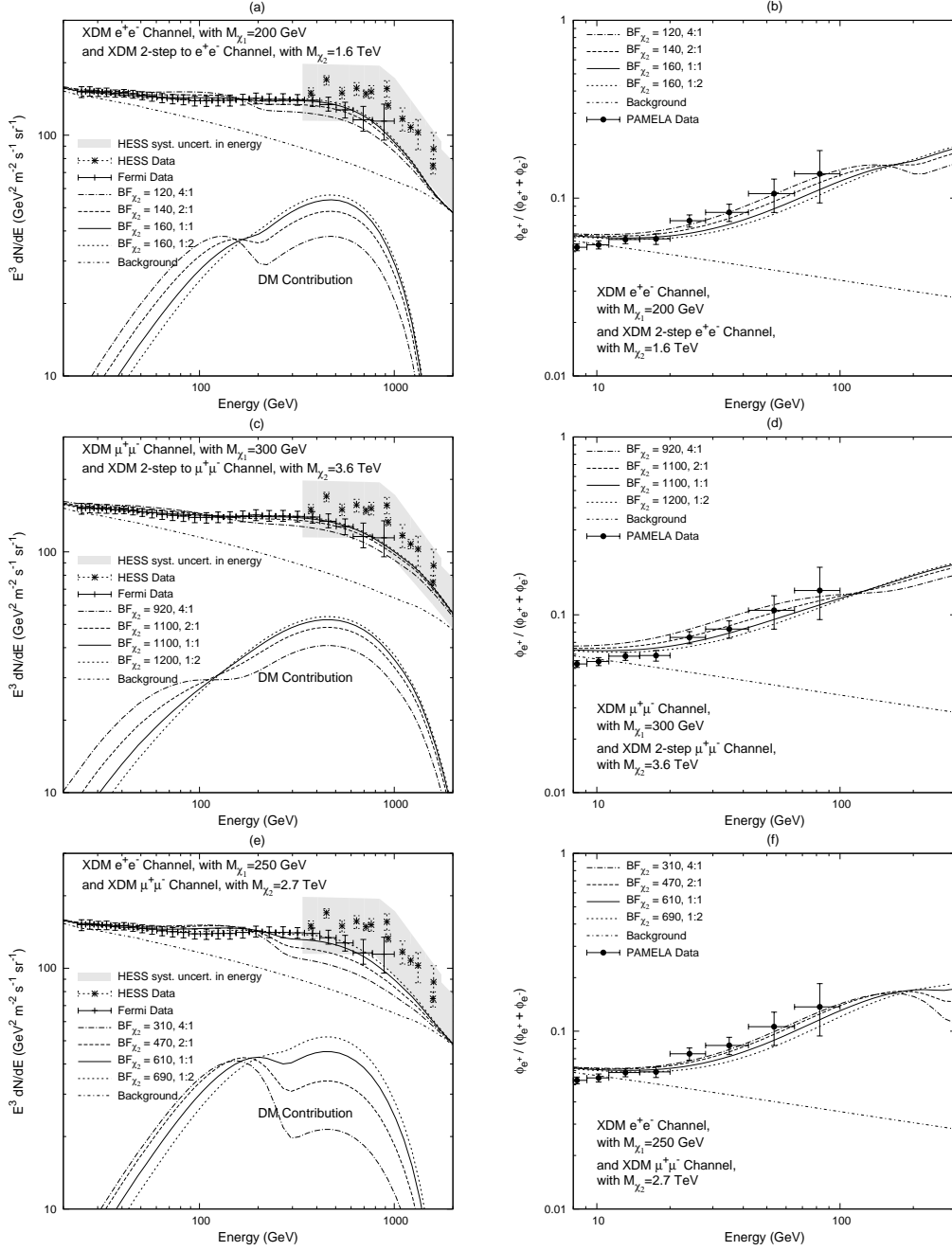


Figure 4: Cosmic ray signals as in Fig. 2. Top: XDM e^\pm with $M_{\chi_1} = 200$ GeV and XDM 2-step to e^\pm with $M_{\chi_2} = 1.6$ TeV. Middle: XDM μ^\pm with $M_{\chi_1} = 300$ GeV and XDM 2-step to μ^\pm with $m_{\chi_2} = 3.6$ TeV. Bottom: XDM e^\pm with $m_{\chi_1} = 250$ GeV and XDM μ^\pm with $m_{\chi_2} = 2.7$ TeV.

4.3 General fits and constraints

In addition to the examples presented, we have also studied a variety of combinations of XDM e^\pm , XDM μ^\pm , XDM π^\pm , XDM 2-step to e^\pm , XDM 2-step to μ^\pm and combinations of XDM to

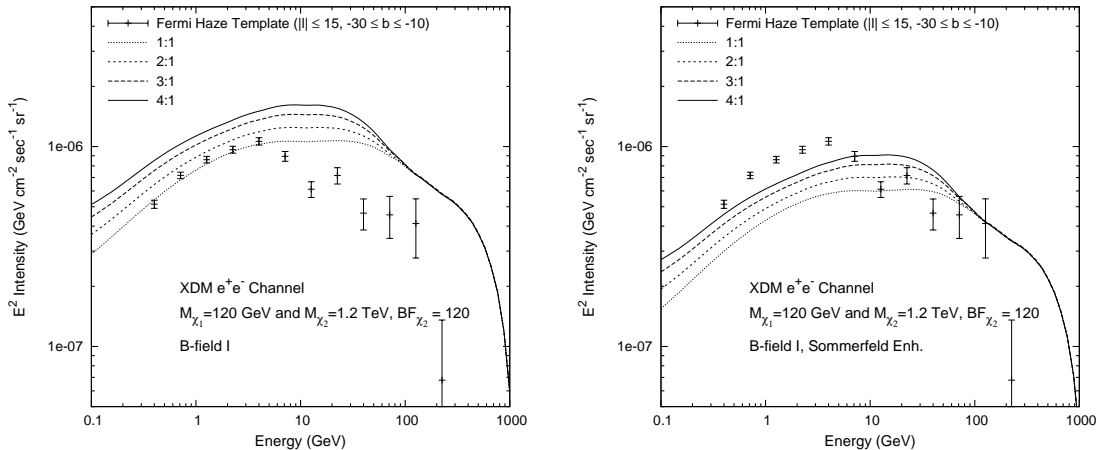


Figure 5: A comparison of the residual Fermi Haze data $|l| < 10^\circ$ and $10^\circ < |b| < 30^\circ$ from [81], versus DM ICS contributions for uniform boost and an Einasto profile (*left*) and with a v^{-1} scaling assuming $v_{disp} \propto r^{-1/4}$ (*right*).

e^\pm and μ^\pm , with various annihilation ratios. In general, for each of these channels we could find a combination of masses M_1 and M_2 , that fit the Fermi $e^+ + e^-$ flux data within 95% C.L. Thus - and not surprisingly - such combinations of two annihilating species fit the Fermi $e^+ + e^-$ data to 95% C.L. in a fairly generic manner.

While we have demonstrated good agreement between the Fermi/PAMELA data sets from MiXDM models, we should consider other constraints as well. A variety of constraints from the diffuse gamma-ray background [82, 83] can arise, but the broad uncertainties in halo models allow the models discussed here to be unconstrained. In contrast, there are limits from the linear regime of the universe and the local halo that more directly connect to the local observations, or do so with fewer uncertainties about galaxy formation.

The most model-independent of these come from the CMB. Recently, [65, 66, 67] have shown the CMB can constrain the maximum annihilation into e^+e^- in the early universe. At $z \sim 10^3$ those electrons will heat and ionize the photon-baryon plasma, changing the power spectrum and the polarization of the CMB. Thus constraints can be put on the annihilation rate at $z \sim 10^3$ based on the WMAP5 data.

Considering that the velocity dispersion of the DM at $z \sim 10^3$ is lower than what we expect locally, those constraints on the DM annihilation can be considered as the saturated values of the Sommerfeld enhancement (although note [84]). [67] have calculated the maximum values of allowed DM annihilations for the XDM e^\pm , XDM μ^\pm and XDM π^\pm channels. In all the cases presented in Fig. 2 to 4 the suggested B.F. are below or similar to the maximum allowed Sommerfeld enhancement allowed by the WMAP5 data. Although there are some additional uncertainties in relating the local signal to that of the early universe (in particular, the local density and contributions from any local substructure), future data from Planck should constrain further the various annihilation channels [67].

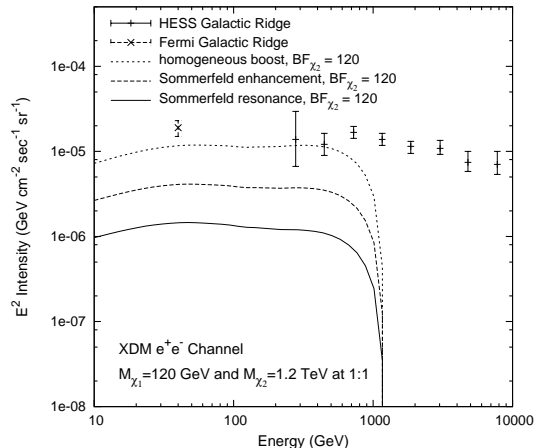


Figure 6: A comparison of the signal from FSR+ICS versus HESS data in the Galactic Ridge, normalized to local PAMELA and Fermi signals assuming a cross section scaling as v^0 , v^{-1} and v^{-2} with $v_{disp} \propto r^{-1/4}$, using an Einasto profile with $\alpha = 0.17$. The lowest data point from Fermi is extracted from the maps of [81].

Dark matter annihilation into charged particles naturally produces high energy γ 's from final state radiation (FSR) which can place strong constraints in the galactic center (GC) and galactic ridge (GR) [85, 86, 87]. These limits have been shown to be generally constraining for models that explain the Fermi electron spectrum [88, 89, 90, 72, 80, 91]. However, this involves an extrapolation into the galactic center, which does involve uncertainties. As a simple example, we include an effect that has been heretofore ignored, namely, the variation in the velocity dispersion v_{disp} as one approaches the galactic center. As noted earlier, many recent simulations with baryons have seen an increase in v_{disp} roughly as $r^{-1/4}$ [33, 34, 35, 36, 37] as one moves to the inner galaxy. As the annihilation enhancement from the long-range force scales as v^{-1} or v^{-2} in resonance regions, this can suppress the signal in the GC and GR.

We show in figure Fig. 6 a comparison between a MiXDM scenario normalized to fit the local cosmic ray data, under the assumption that the cross section is unchanged in the inner galaxy, or under the assumption that it has changed from the higher velocities. As is clear from the figure, these effects easily allow consistency with the HESS constraints. At the same time, the signal in the Haze region is only affected by a factor of 1.6 or 2.4 for v^{-1} or v^{-2} , respectively. Of course, these curves assume extrapolation of a functional form for halo and velocity dispersion into regions that are not probed by simulations, and thus should be taken with a grain of salt³.

³In this analysis, we are scaling the cross section as $\langle\sigma v\rangle \propto r^{-1/4}$ or $r^{-1/2}$. Once $\pi\alpha/v \sim 1$, this effect saturates. Even in the resonance case, this does not become relevant until the inner \sim pc, and does not affect the plots shown.

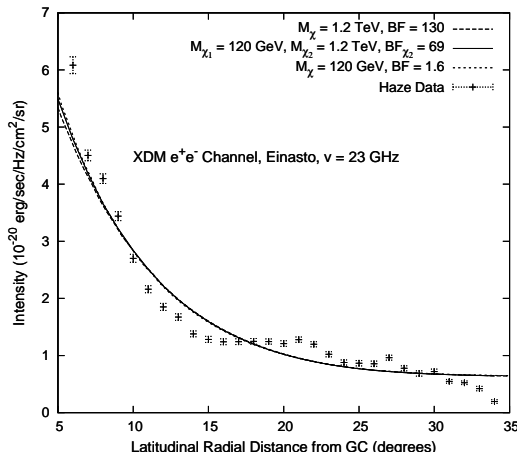


Figure 7: Synchrotron radiation at 22.5 GHz from e^\pm of DM origin fitted to the microwave Haze of the same frequency. (*Solid line*): flux from the two XDM e^\pm species with masses 120 GeV and 1.2 TeV, and relative annihilation rates of 1:1. (*Dashed line*): fit of the 1.2 TeV only. (*Dotted line*): equivalent fit for 120 GeV only.

5. Counting the number of WIMP species with Synchrotron radiation

One of the elements of the case for WIMP annihilation comes from the microwave excess in the galactic center, i.e. the “microwave Haze” [92, 93, 9]. Such data have already been used to constrain the possible models that might explain it [93]. Should Planck extend these data clearly to higher frequencies, it may serve to allow an additional handle on the details of WIMP annihilation.

To study this, we shall primarily use the simplified model shown in Fig. 2 (XDM e^\pm with $M_{\chi_1} = 120\text{GeV}$ and $M_{\chi_2} = 1.2\text{TeV}$, with relative annihilations of 1:1).

Before proceeding to the complete analysis, let us begin by studying the microwave Haze data we already have. As we show in Fig. 7 just using the 22.5 GHz WMAP band where the microwave Haze error bars are the smallest⁴, it is not possible to distinguish between the cases where there is one mass of $M_\chi=1.2$ TeV from the MiXDM case of two 120 GeV / 1.2 TeV. This is not surprising, as e^\pm that emit synchrotron radiation at 22.5 GHz have energies between $5 \lesssim$ to 50 GeV, so e^\pm originating from both species contribute essentially equally.

5.1 Modeling Synchrotron Emission with Power Laws

As we discuss in the appendix, in considering the emissivity $j(\nu)$ in the range of ~ 100 GHz, one should expect the synchrotron emissivity $J_1(\nu)$ of the full distribution of e^\pm that originate from χ_1 (with $M_{\chi_1} = 120$ GeV) to be described by a steeper power law than that of χ_2 (with $M_{\chi_2} = 1.2$ TeV),

$$J_1(\nu) \sim \nu^{-\alpha_1}, \quad J_2(\nu) \sim \nu^{-\alpha_2} \quad \text{with } \alpha_1 > \alpha_2, \quad (5.1)$$

⁴not including the CMB bias

simply because there is more energy in high energy electrons from χ_2 to contribute to the higher frequencies. That is also shown in Fig. 8 where we present the synchrotron radiation from the e^\pm of DM origin vs latitude for ν : 70, 143, 353 and 857 GHz (frequencies to be measured by Planck). The calculated values of the synchrotron radiation are averaged over longitudes of -10° to $+10^\circ$ as the WMAP microwave Haze is calculated from that region of the sky [94]. The annihilation cross sections for those particles are fixed by fitting to the 22.5 GHz WMAP microwave Haze shown in Fig. 7. As explained, the synchrotron emissivity of e^\pm from a 120 GeV DM particle drops faster than that of a 1.2 TeV DM particle.

Note that in Fig. 7 we fit the 22.5 GHz microwave Haze band data with a combination of the synchrotron radiation from the e^\pm of DM origin and an extra constant offset, as the overall zero of the microwave Haze is somewhat uncertain. In Fig. 8 instead we present only the synchrotron radiation from the e^\pm of DM origin, but it should be expected that with actual data some constant offset will be required.

As a result of eq. 5.1 the combination distribution in the 2-species case will be described by a power law $J_{comb} \sim \nu^{-\alpha_{comb}}$ of intermediate steepness.

$$J_{comb}(\nu) \sim \nu^{-\alpha_{comb}} \text{ with } \alpha_1 > \alpha_{comb} > \alpha_2 . \quad (5.2)$$

The key point in (5.2), is that $\alpha_1 \neq \alpha_2$. While this may appear obvious, there are actually subtleties involved that we shall explain. The obvious element is the direct relationship between synchrotron spectrum and the hardness of the electron spectrum. From synchrotron theory we know that for a power law distribution of electron energies of the form $N(E) = \kappa E^{-p}$, the synchrotron emissivity of the distribution goes as [95]:

$$J(\nu) \propto \kappa \nu^{-(p-1)/2} . \quad (5.3)$$

Considering that for both masses we used the same annihilation channel, one would think that $J_1(\nu)$ and $J_2(\nu)$ should be described by the same power law, which is true - up to a point. The injection spectra are given by the same formula [9] which gives an injection power law of 0, and the dominant energy losses (synchrotron and ICS) scale as $\frac{dE}{dt} \propto E^{-2}$. However, eq. (5.3) neglects the energy cut-off E_{cf} in the distribution of the electrons. As we explained earlier in this section, it is exactly the presence of the cut-off that for frequencies $\nu \ll \nu_{cf}$ (5.3) where:

$$\nu_{cf} = \frac{3}{2} \frac{e B E_{cf}^2}{2 \pi m_e^3} \sin \alpha , \quad (5.4)$$

shouldn't be applied blindly. Thus $\alpha_1 \neq \alpha_2$.

A second element contributing to $\alpha_1 > \alpha_2$ is that the Thompson approximation of the cross-section of ICS from optical starlight breaks down at electron energies $E \sim 100$ GeV, with the actual cross section between the electron and the photon being described by the Klein-Nishina cross section [95]:

$$\sigma_{K-N} = \frac{3}{8} \sigma_T x^{-1} \left\{ \left[1 - \frac{2(x+1)}{x^2} \right] \ln(2x+1) + \frac{1}{2} + \frac{4}{x} - \frac{1}{2(2x+1)^2} \right\} , \quad (5.5)$$

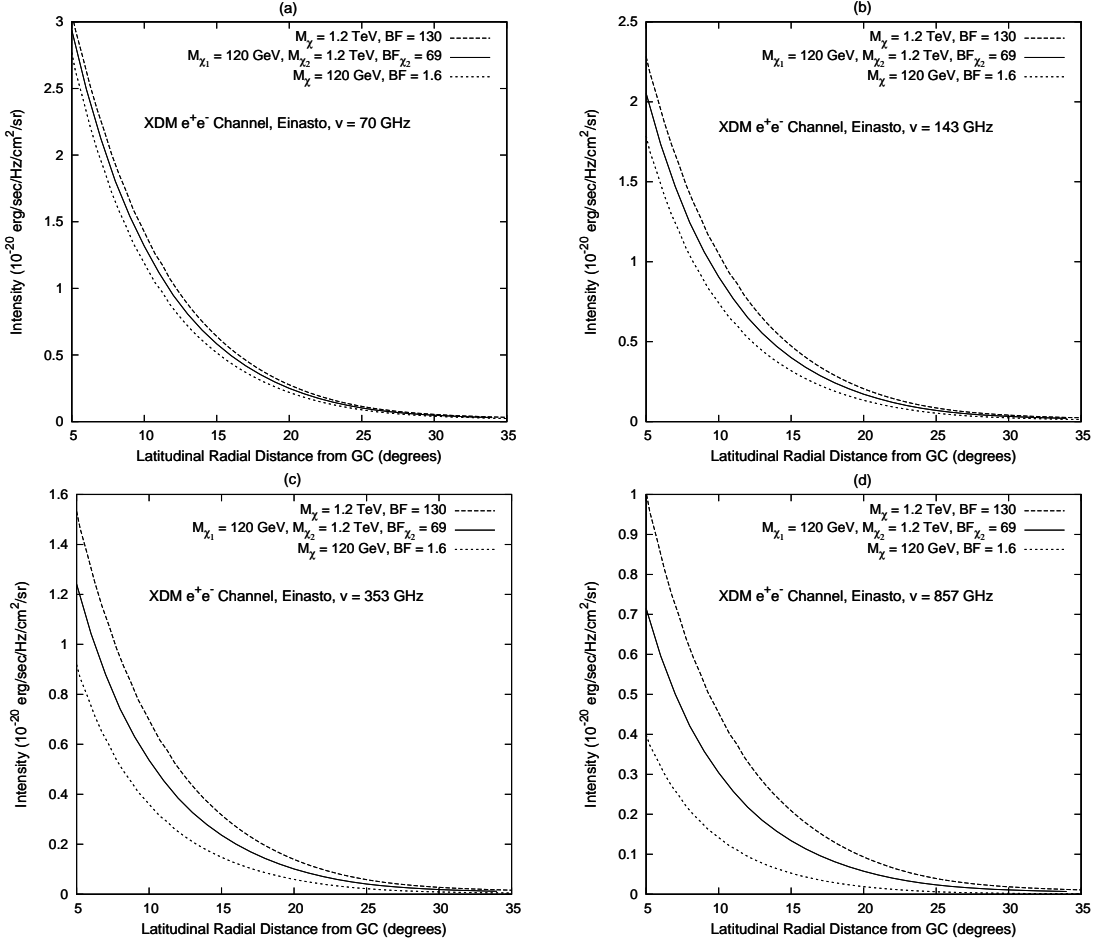


Figure 8: Synchrotron radiation from the e^\pm of DM origin as in Fig. 7, for 70 GHz (top left), 143 GHz (top right), 353 GHz (bottom left) and 857 GHz (bottom right). Boost factors are from fitting to the 22.5 GHz microwave Haze.

where $x = \frac{\hbar\omega}{m_e c^2}$. At the limit where $x \gg 1$ equation 5.5 simplifies to:

$$\sigma_{K-N} = \frac{3}{8} \sigma_T x^{-1} \left(\ln(2x) + \frac{1}{2} \right). \quad (5.6)$$

This results in an energy loss rate $\frac{dE}{dt}$ due to ICS from optical starlight that scales as E^β with $\beta < 2$ and gradually decreasing with increasing electron energy E . As a consequence, ICS is a less efficient energy loss for the higher energy electrons, resulting in more energy (fractionally) being lost to synchrotron radiation, and a harder synchrotron spectrum.

In Fig. 9 we show the ratio of synchrotron radiation flux at frequency ν averaged between 6° to 15° in latitude and -10° to $+10^\circ$ in longitude (microwave Haze region), to the same averaged flux at 22.5 GHz.

$$\frac{\int J(\nu) d\Omega dr}{\int J(\nu=22.5 \text{ GHz}) d\Omega dr}, \quad (5.7)$$

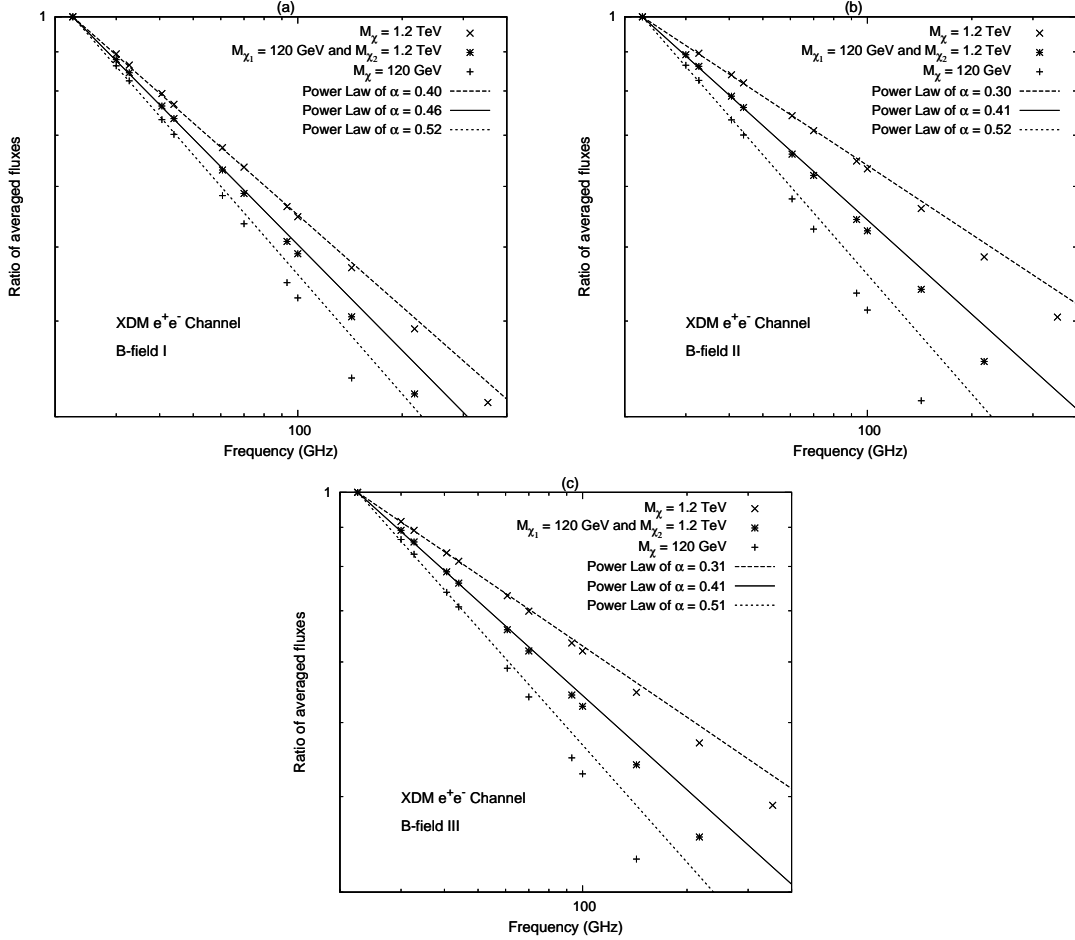


Figure 9: Plot (a): Ratio of synchrotron radiation at frequency ν over radiation at 22.5 GHz from e^\pm of DM origin. Assumed magnetic field model: “B-field I” (*Solid line*): ratio for the two XDM e^\pm species with masses 120 GeV and 1.2 TeV, at $(\chi_1:\chi_2)$ of 1:1. (*Dashed line*): ratio for the 1.2 TeV only. (*Dotted line*): equivalent ratio for 120 GeV only. Plot (b): Same as for (a) but with magnetic field model “B-field II”. Plot (c): Same as (a) but with magnetic field model “B-field III”.

where dr refers to the integration over the line of light and $d\Omega$ to the integration over the sky region. That ratio is calculated for the cases of XDM e^\pm channel with $M_\chi = 120$ GeV, $M_\chi = 1.2$ TeV separately as well as the MiXDM case. We use the 5 WMAP frequencies: 22.5, 32.7, 40.6, 60.7 and 93.1 GHz [96] and the 9 Planck frequencies 30, 44, 70 GHz (measured from the Low Frequency Instrument)[97, 98] and 100, 143, 217, 353, 545 and 857 GHz (measured from the High Frequency Instrument)[99, 100]. We also show the indices of the power laws that fit our calculations from the lowest frequency (22.5 GHz) up to ~ 100 GHz, where deviations from the one power law description arise.

Based on (5.2) if we are able to measure the power law index α of $J(\nu)$, and if we know the mass M_χ (or M_{χ_2} for the 2-mass case) and the annihilation channel via which e^\pm are produced

then we can discriminate between the 2-species χ_1, χ_2 case and the case where there is only χ_2 in nature. As shown in Fig. 9a⁵, the power law for frequencies up to ~ 100 GeV, is for the case of a single species $M_\chi = 1.2$ TeV equal to $\alpha = 0.40$ while for the 2-species case with $M_{\chi_1} = 120$ GeV and $M_{\chi_2} = 1.2$ TeV it is $\alpha = 0.46$, because of the contribution from χ_1 that falls with a steeper power law ($\alpha = 0.52$). Also in Fig. 9 notice that at ν greater than ~ 100 GHz, the power-law approximation of the e^\pm distribution stops being valid.

In general, for the MiXDM scenario in which masses are separated by an order of magnitude or greater, the difference in the power law index compared to the single WIMP cases is $\simeq 0.1$ or greater. There are many uncertainties and challenges in extracting the Haze from future Planck data, so it remains to be seen whether this will be adequate. In this paper we do not intend to discuss the uncertainties arising from understanding the various astrophysical contributions (free-free emission, synchrotron radiation from primary electrons and thermal and spinning dust)[101, 94]. Currently only the 22.5 and 32.7 GHz from WMAP have small enough error bars to be used in order to calculate the power law α . In [93], the authors find that the ratio of the averaged Haze flux at 22.5 GHz to that at 32.7 GHz is $J(22.5GHz)/J(32.7GHz) \approx 1.18 \pm 0.10$ that gives a range, $0.2 < \alpha < 0.6$. Since [93] used only the statistical errors of the microwave Haze, while there are additional large uncertainties arising predominantly from the microwave Haze's correlation with the CMB. Thus the actual range of values of α from the microwave Haze is even greater than this. At the moment, one- and two- species scenarios are indistinguishable within errors.

Another difficulty in determining whether we are in a MiXDM scenario is the uncertainty in the annihilation channel, itself. Constraints from fitting the Fermi/HESS electron data require $1 \text{ TeV} \lesssim M_{\chi_2} \lesssim 4 \text{ TeV}$, depending on the annihilation mode, with some significantly softer than others. Such changes will clearly impact the spectrum of the synchrotron emission $J(\nu)$. To explore this, we show in Fig. 10 the ratio of synchrotron radiation flux at frequency ν (normalized to 22.5 GHz) averaged over the microwave Haze region (as in Fig. 9) for four different annihilation channels for single species of mass M_χ . Those four channels are XDM e^\pm , XDM μ^\pm , XDM 2-step cascade to e^\pm and XDM 2-step cascade to μ^\pm . The values for M_χ coincide with the values of M_{χ_2} used in Fig. 4, so give good fits to the Fermi data.

As one can see from Fig. 10a (B-field I) the power laws describing $J(\nu)$ until ~ 100 GHz, vary between:

$$0.4 \leq \alpha \leq 0.46 . \tag{5.8}$$

The channel XDM π^\pm [73] is not shown in Fig. 10, but gives $\alpha = 0.43$ (for $M_\chi = 3.1$ TeV). Thus any channel that can be thought (with respect to the injection spectrum of the produced e^\pm) as a combination of XDM e^\pm , μ^\pm and π^\pm will have a power law in the region of (5.8), provided χ can fit the Fermi data and not violate the HESS upper limits⁶.

⁵See section 5.2 for definitions of magnetic fields

⁶ τ^\pm channels can fit the local e^\pm spectra, but are constrained from diffuse γ -rays, and we do not consider those modes.

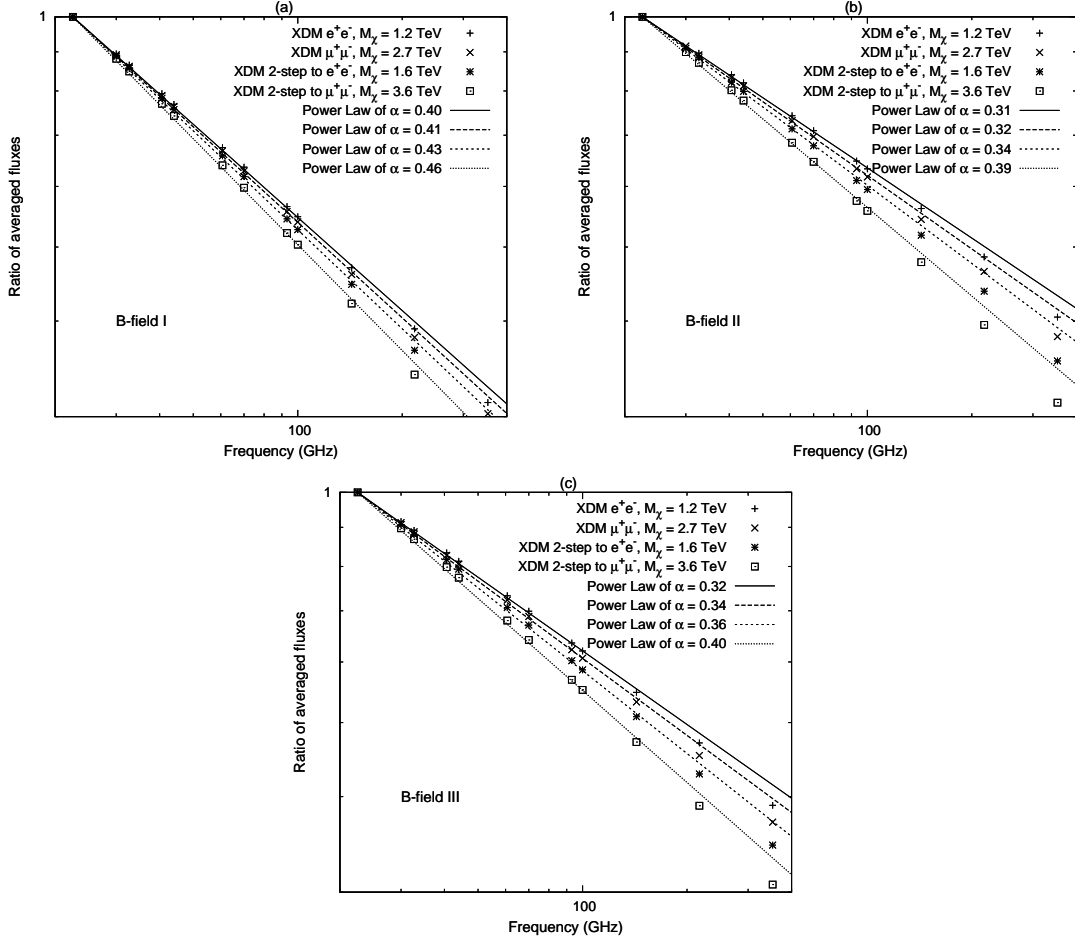


Figure 10: Plot (a): Ratio of synchrotron radiation as in 9a (used magnetic field model: “B-field I”). (Solid line): ratio for the XDM e^\pm species with $M_\chi = 1.2$ TeV. (Long dashed line): ratio for the XDM μ^\pm species with $M_\chi = 2.7$ TeV. (Short dashed line): ratio for the XDM 2-step cascade to e^\pm species with $M_\chi = 1.6$ TeV. (Dotted line): ratio for the XDM 2-step cascade to μ^\pm species with $M_\chi = 3.6$ TeV. Plot (b): Same as in (a) with magnetic field model “B-field II”. Plot (c): Same as in (a) with magnetic field model “B-field III”.

The region of (5.8) is quite narrow⁷, making it a challenge to determine the mass and the annihilation channel based on the microwave Haze data only. Yet this information can be used in understanding the nature of DM. To do this, we will require an accurate measurement of the microwave Haze at frequencies ~ 100 GHz, which is challenging due to the various uncertainties involved in subtracting the astrophysical backgrounds and the CMB from the WMAP and Planck data.

⁷That is expected from the fact that $\alpha \sim (p - 1)/2$ with p the index to the spectrum of the electrons responsible for the radiation (see (5.3))

5.2 Dependence of the B-field vs ISRF assumptions

From the Eq. B.1 we know that the synchrotron emissivity $j(\nu)$ of an electron inside a magnetic field is proportional to the amplitude of the B-field. If the microwave Haze can be explained from DM, then the region of the Galaxy that provides the major contribution to it is $1 < r < 2$ kpc. For that region there are significant uncertainties in the literature about the value of the B-fields amplitude and shape(see [102, 103, 104, 105, 106, 107, 108] and [109] among others).

To study the effects of the uncertainties of the B-field amplitude, we follow [74] and use variants of the default magnetic field profile from GALPROP:

$$B(\rho, z) = B_0 \exp\left(\frac{R_\odot - \rho}{\rho_c}\right) \exp\left(-\frac{z}{z_c}\right). \quad (5.9)$$

with $B_0 = 5\mu G$ being the value for the total(combined random and large scale “ordered”) local value of the magnetic field, $R_\odot = 8.5\text{kpc}$, ρ_c and z_c being the characteristic scales along ρ and z directions respectively. We used three options for the values of ρ_c and z_c .

1. $\rho_c = 4.5\text{kpc}$ and $z_c = 2.0\text{kpc}$, defined as “B-field I”,
2. $\rho_c = 10.0\text{kpc}$ and $z_c = 2.0\text{kpc}$, defined as “B-field II” and
3. $\rho_c = 10.0\text{kpc}$ and $z_c = 4.0\text{kpc}$, defined as “B-field III”.

The magnetic field model defined as “B-field I”, provides agreement with the 408 MHz Haslam map[110, 111], while the model defined as “B-field II”, is the “conventional” galprop assumption. “B-field III” was chosen to take into consideration uncertainties in the scale height z_c of the magnetic field⁸. In generating the plots shown in Fig.8, we used the “B-field I” model.

In Fig. 9b and c and in Fig.10b and c, we show the dependence of the magnetic field on the ratio of synchrotron radiation for the cases studied in Fig. 9a and 10a. We can see that for the cases where $\rho_c = 10\text{kpc}$, the power-law spread is greater than that of $\rho_c = 4.5\text{kpc}$. In the case of $\rho_c = 10\text{kpc}$, the magnetic field at $1 < z < 2$ (kpc) is weaker by a factor of 2, compared to that of the $\rho_c = 4.5\text{kpc}$ case, thus the power in synchrotron radiation is by a factor of 4 lower. As explained previously, one reason for the difference in the observed power-laws is the fact that ICS losses compete with synchrotron losses. Lower synchrotron radiation losses result in ICS losses being more important⁹. Thus the difference in the observed power-laws shown in 9b and c(10b and c) vs 9a (10), is enhanced.

Moreover, the weaker magnetic fields shown in 9b and c(10b and c) versus that shown in 9a (10a) results in a lower power-law values for α . This simply arises because of the lower total synchrotron energy losses (as we keep our ISRF constant) resulting in a smaller depletion of the higher energy electrons.

⁸Values of $z_c \simeq 1\text{kpc}$ have been used by [102] and [103]. Such a low scale height for the magnetic field would result in a greater spread of power-laws as those presented in Fig. 9 and 9, and thus would make it easier to separate among different scenarios.

⁹ $\frac{dE}{dt}_{ICS}$ is greater
 $\frac{dE}{dt}_{total}$

As we see the current uncertainties in the B-field are significant enough to make an analysis based solely on the observed power-laws α degenerate among the various DM models. The ISRF and as well the diffusion properties of the electrons are also not well modeled yet, adding additional uncertainties. Yet, as diffusion models improve and are better constrained, and as more accurate measurements of the ISRF and the B-field in the regions of interest appear, these uncertainties will diminish. Furthermore, one would hope that in these scenarios, we may have some estimate of the(some) DM species from direct searches, or other indirect data. Thus, in concert with such results, such an analysis as we have described would be a complementary tool for understanding the Dark sector.

6. 3 masses

Of course, once two masses are present, we can consider more, and even heavier DM species. We will confine our discussion to the case where there are three DM species and refer to species χ_1 as the lightest, χ_2 as the intermediate mass species and χ_3 as the heaviest species.

$$M_{\chi_1} < M_{\chi_2} < M_{\chi_3} . \quad (6.1)$$

As explained in section 2.1 the three species are expected to have similar fluxes of e^\pm at $E \lesssim M_{\chi_1}$.

A scenario where the three particles are spaced within 100 GeV-3 TeV is essentially indistinguishable from the two-mass case. A scenario where $M_{\chi_1} \sim 10$ GeV would be difficult to be seen from the e^\pm flux, as Solar modulation is significant at $E \lesssim 10$ GeV, so e^\pm fluxes at those energies can't be measured accurately. For instance, [21] considered a case of two masses where the lightest at 3 – 10 GeV is suggested in order to explain via its elastic scattering to NaI target the annual modulation signal measured DAMA/LIBRA [112], but such a scenario would be difficult to extract from the signals we have discussed. We do note, however, that such a light WIMP could, in principle, produce an additional component of electrons that could contribute to the low energy Fermi Haze, although additional astrophysical sources may contribute as well.

The most interesting from the point of view of locally measured e^\pm fluxes is the case where:

$$M_{\chi_1} \sim 100\text{GeV} , M_{\chi_2} \sim 1\text{TeV} \text{ and } M_{\chi_3} \sim 10\text{TeV} . \quad (6.2)$$

where additional contributions at the highest energy can arise.

In Fig. 11 we present the case of a $M_{\chi_1} = 200$ GeV annihilating through XDM e^\pm channel, $M_{\chi_2} = 1.0$ TeV XDM e^\pm channel as well and a $M_{\chi_3} = 8.0$ TeV annihilating through 2-step cascade to muons. We note that even though there is good agreement to the Fermi data, the projected positron fraction is below the one measured by PAMELA by almost a factor of two.

While the two-mass case can be easily realized, the three-mass case described by (6.2) is actually allowed only with very specific annihilation modes. The reason behind that is the existence of the HESS $e^+ + e^-$ upper limits[5, 6], that suggest a turn-off of the source

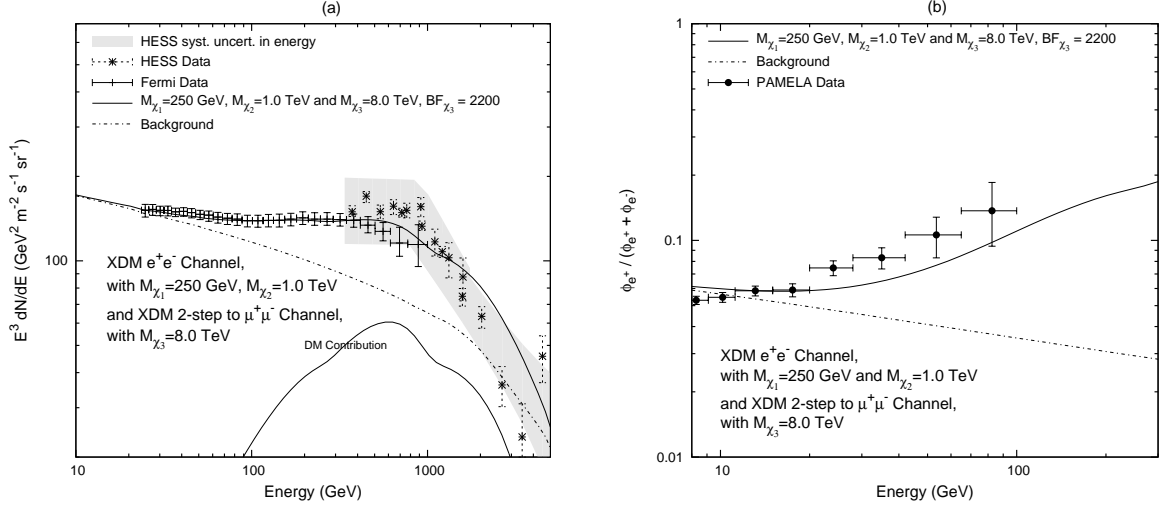


Figure 11: Fitted $e^+ + e^-$ spectra as in Fig. 2 for annihilation of 3 XDM species with $M_{\chi_1} = 250$ GeV, $M_{\chi_2} = 1.0$ TeV through e^\pm channel and $M_{\chi_3} = 8.0$ TeV through 2-step cascade to μ^\pm .

of e^\pm responsible for the excess compared to the conventional backgrounds at ~ 1 TeV. (A change in the background power law at ~ 1 TeV would also be a reasonable possibility.) As a $M_{\chi_3} \sim 10$ TeV would in general create significant fluxes of e^\pm at ~ 1 TeV, unless the annihilation mode is adequately soft, there are conflicts with the HESS upper bounds.

Going to higher than $M_{\chi_3} \sim 10$ TeV these tensions are aggravated, as the propagated e^\pm contribute to the e^\pm flux with $E < 5$ TeV. The local primary electron flux at energies $E \gtrsim 1$ TeV is mainly influenced by local and recent SN explosions[113, 114, 115, 116, 117, 118], and very young pulsars[119, 120, 121, 122, 68, 69] as well. These uncertainties make a detection of a heavier mass difficult in the e^\pm data.

7. Scattering and Effects on the DM Halo

The presence of “long-range” forces in the dark sector can be constrained from the stability of DM halos [123, 124] and other properties of galaxies [124, 125, 126]. However in the context of MiXDM there is an intriguing twist. It is possible that the heavy WIMP could have a lower scattering rate than the lighter WIMP. This may be because of the different mass splittings δ , or the different m_ϕ/m_χ , or, possibly, because the WIMPs couple to different force carriers. There are other possibilities, for instance that there are other nearby states, or that there is a residual symmetry allowing degenerate excited states with a long range force between them (analogous to the charged wino, for instance), in which case these light WIMPs might scatter very frequently. Such scatterings can easily be strong within the dark sector without leading to a significant WIMP-nucleus interaction, as was explored in [32].

In such a case, if the light WIMP scattering rate is large enough while leaving the heavier WIMP scattering rate small enough, the light WIMP halo would collapse, leading to a completely non-Maxwellian velocity distribution. Since this WIMP is only 1% of the total

energy density, however, this effect would be of little consequence for the total halo. On the other hand, the consequences for direct detection experiments would be profound. The number density and velocity distribution of the lighter WIMPs locally would change significantly, with possibly only the highest velocity particles which are just now falling into the Milky Way present in the event that the light halo has collapsed. In such a case, the lightest WIMP might dominate the annihilation signal from the inner galaxy, while the heavier WIMP would dominate the local cosmic ray signals.

It is not clear how to approach this quantitatively, except to recognize that in MiXDM scenarios the velocity and density structure of the subdominant species can be radically altered, with the subsequent consequences for direct and indirect detection experiments.

8. Conclusions

Cosmic ray signals from PAMELA and Fermi among other have prompted a reexamination of our assumptions of the nature of dark matter. Two of the most central are the assumptions that annihilations are into standard model states, and that there is a single parity, namely R-parity, that stabilizes the WIMP.

Relaxing the latter opens the possibility that the dark matter is composed of multiple particles, with different masses and relic abundances. Such a scenario has been previously motivated to explain both DAMA and INTEGRAL. We have argued that such a “MiXDM” scenario, in which DM annihilates as in standard XDM into light force carriers can naturally lead to similar annihilation rates, even if the different WIMP relic densities are different by an order of magnitude. The consequence is to modify possible particle physics interpretations of the spectra. Softer spectra can arise naturally from the presence of the second, lighter WIMP state, while even bumps and dramatic spectral features can arise in the positron and electron spectra from the presence of these lighter states.

We find that these models are in good agreement with the Fermi $e^+ + e^-$ flux and the PAMELA positron fraction, with the heaviest mass restricted by the HESS upper bounds. These cross sections are very similar to what is needed to explain microwave and gamma-ray excesses in the inner galaxy region, while still below bounds from the CMB. Limits from the Galactic Ridge, while possibly constraining, are weakened when velocity-dependent effects are taken into account.

The presence of the lighter state is possibly detectable in a variety of ways. Beyond the possible features in the e^+ and e^\pm spectra, the changes in the synchrotron emission spectrum can also help distinguish it. In particular, synchrotron radiation from e^\pm of DM origin at frequencies up to ~ 500 GHz, probed by Planck, are potentially different for these models. Unfortunately, the uncertainties in the magnetic field, ISRF and electron diffusion, as well as the great number of possible particle physics models, currently it is not possible to discriminate from synchrotron emission alone between a one DM and a two DM species scenarios that both fit the PAMELA and Fermi data. Yet, when combined with a better understanding of all the factors involved in the calculations of the microwave Haze and the

synchrotron radiation(B-field, ISRF, diffusion models, dust emission, Planck instrumental errors), such a tool may offer an important handle, especially in combination with other indirect and direct DM searches.

Interesting additional possibilities exist as well. One can consider a third, heavier WIMP, although we find that its effects are highly constrained by the HESS electron limits, and that it is difficult to generate any features at high energies consistent with data. A possibility exists for subdominant components to have very large scattering rates, potentially collapsing the lighter WIMP halo, and radically altering the predictions for direct detection scattering rates.

Acknowledgments The authors would like to thank Nima Arkani-Hamed, Gregory Dobler, Douglas Finkbeiner, Joseph David Gelfand, Lisa Goodenough, Ronnie Jansson, Dmitry Malyshev, Tracy Slatyer and Itay Yavin for fruitful discussions. NW is supported by DOE OJI grant # DE-FG02-06ER41417 and NSF CAREER grant PHY-0449818. IC is supported by DOE OJI grant # DE-FG02-06ER41417 and also by the Mark Leslie Graduate Assistantship.

A. DM Halo and CR propagation

For all our calculations we considered an Einasto profile using the parametrization of [127]:

$$\rho(r, z) = \rho_0 \exp \left[-\frac{2}{\alpha} \left(\frac{r^\alpha - R_\odot^\alpha}{r_{-2}^\alpha} \right) \right], \quad (\text{A.1})$$

with $\alpha = 0.17$, $r_{-2} = 25 \text{ kpc}$ and $R_\odot = 8.5 \text{ kpc}$. We considered the local DM mass density to be $\rho_0 = 0.4 \text{ GeV cm}^{-3}$ that is in agreement with calculations of the local dynamical mass based on Hipparcos data and the estimates on the local baryonic mass[128, 129, 130, 131] and also with [132].

While we assume that our boost from the thermal cross section is purely from particle physics, substructure in the distribution of DM can also exist, affecting the amplitude and spectrum of the signal. For instance, [133, 134, 73] find that substructure can create spectral hardening of the propagated e^\pm spectrum at high energies. If such substructure gives a significant contribution to the local e^\pm flux, it would also enhance the bumps at $E \sim M_{\chi_1}$, although this depends on particle physics and astrophysics parameters.

To determine the cosmic ray properties, we have calculated the propagation of the e^\pm in the Galaxy using GALPROP[135]. In our models for the background e^\pm fluxes we have considered a magnetic field of a local value of $5 \mu\text{G}$ with a peak value of $33 \mu\text{G}$ in the galactic center, and the standard GALPROP Interstellar Radiation Field (ISRF)[136]. For the diffusion of the CRs galprop considers a diffusion zone within which the spatial diffusion coefficient is considered homogeneous in space depending on rigidity as:

$$D_{xx} = \beta D_{0xx} \left(\frac{R}{D_{\text{rigid br}}} \right)^{D_g}, \quad (\text{A.2})$$

with $\beta = v/c$, $R = \frac{p}{q}$ the rigidity, D_{0xx} diffusion coefficient at reference rigidity $D_{rigidbr}$ and D_g diffusion index. Our assumptions for D_{0xx} and δ provide good agreement with proton, He, C, Fe, B/C and subFe/Fe fluxes, as well as antiproton over proton ratio[73]. For a more extensive discussion of background electrons and positrons one can refer to [135, 9, 137].

We also define the boost factor that we are going to refer to as just the overall enhancement in the $\sum_i n_i^2 \langle \sigma_i | v \rangle$ needed to fit the data at hand compared to its value assuming an Einasto profile with $\rho_0 = 0.4 GeV cm^{-3}$ and thermally averaged cross sections such that the total relic mass density agrees with the current constraints from WMAP, on $\Omega h^2 = 0.1099 \pm 0.0062$ [138].

For the case of $M_{\chi_1} \ll M_{\chi_2}$ and for an Einasto profile as we use in this paper, we can simply write the B.F. as just¹⁰:

$$B.F. \approx \frac{\langle \sigma_2 | v \rangle_{Fitted}}{3 \times 10^{-26} cm^3 s^{-1}}, \quad (A.3)$$

as χ_1 contributes only $\sim \frac{M_{\chi_1}^2}{M_{\chi_2}^2}$ to the relic mass density. In our calculations we took into account corrections in the relic density that scale with the logarithm of the masses M_χ

B. Review of Synchrotron Emission

The emissivity of a single electron to synchrotron radiation is given by[95]:

$$j(\nu) = \frac{\sqrt{3}e^3 B \sin \alpha}{8\pi^2 \epsilon_0 c m_e} \frac{\nu}{v_c} \int_{\nu/v_c}^{\infty} K_{5/3}(z) dz \quad (B.1)$$

where B is the magnetic field and α the angle between the B-field and the velocity of the electron, $K_{5/3}$ is the modified Bessel function of the second kind of order 5/3 and v_c is the critical frequency:

$$v_c = \frac{3}{2} \gamma^2 \frac{eB}{2\pi m_e} \sin \alpha. \quad (B.2)$$

which scales as $\propto \gamma^2$, as the gyroradius of the electrons in the ISM is $\propto \gamma$. The maximum value of $j(\nu)$ is at $\nu_{peak} = 0.286 v_c$, at $\nu = 3.38 v_c$ the $j(\nu)$ has 1/10 of its peak value, while at the very low and very high frequency limits it is given by:

$$j(\nu) = \frac{\sqrt{3}e^3 B \sin \alpha}{8\pi^2 \epsilon_0 c m_e} \times \left\{ \begin{array}{l} \frac{4\pi}{\sqrt{3}\Gamma(1/3)} \left(\frac{\nu}{2v_c} \right)^{1/3} \text{ for } \nu \ll v_c \\ \left(\frac{\pi\nu}{2v_c} \right)^{1/2} \exp\left(-\frac{\nu}{v_c}\right) \text{ for } \nu \gg v_c \end{array} \right\} \quad (B.3)$$

Considering the exponential cut-off at frequencies much higher than the critical frequency we can see that at the highest frequencies to be probed by Planck (up to 857 GHz), the less energetic electrons are not going to emit significant synchrotron radiation. For instance, for a $\simeq 50$ GeV electron, and a magnetic field of $\simeq 20 \mu G$ such as expected in the Haze region, the critical frequency is, $v_c \simeq 1$ THz, thus its emissivity peaks at 300 GHz. A 1 TeV electron though has for the same B-field a critical frequency of $v_c \simeq 400$ THz thus the emissivity peaks at $\simeq 120$ THz.

¹⁰within logarithmic corrections on M_{χ_2}

References

- [1] **PAMELA** Collaboration, O. Adriani *et al.*, *An anomalous positron abundance in cosmic rays with energies 1.5–100 GeV*, *Nature* **458** (2009) 607–609, [[arXiv:0810.4995](#)].
- [2] **The Fermi LAT** Collaboration, A. A. Abdo *et al.*, *Measurement of the Cosmic Ray e^+ plus e^- spectrum from 20 GeV to 1 TeV with the Fermi Large Area Telescope*, *Phys. Rev. Lett.* **102** (2009) 181101, [[arXiv:0905.0025](#)].
- [3] J. Chang *et al.*, *An excess of cosmic ray electrons at energies of 300–800 GeV*, *Nature* **456** (2008) 362–365.
- [4] **PPB-BETS** Collaboration, S. Torii *et al.*, *High-energy electron observations by PPB-BETS flight in Antarctica*, [arXiv:0809.0760](#).
- [5] **H.E.S.S.** Collaboration, F. Aharonian *et al.*, *The energy spectrum of cosmic-ray electrons at TeV energies*, *Phys. Rev. Lett.* **101** (2008) 261104, [[arXiv:0811.3894](#)].
- [6] H. E. S. S. C. F. Aharonian, *Probing the ATIC peak in the cosmic-ray electron spectrum with H.E.S.S.*, [arXiv:0905.0105](#).
- [7] N. Arkani-Hamed, D. P. Finkbeiner, T. R. Slatyer, and N. Weiner, *A Theory of Dark Matter*, *Phys. Rev.* **D79** (2009) 015014, [[arXiv:0810.0713](#)].
- [8] D. P. Finkbeiner and N. Weiner, *Exciting Dark Matter and the INTEGRAL/SPI 511 keV signal*, *Phys. Rev.* **D76** (2007) 083519, [[astro-ph/0702587](#)].
- [9] I. Cholis, L. Goodenough, and N. Weiner, *High Energy Positrons and the WMAP Haze from Exciting Dark Matter*, *Phys. Rev.* **D79** (2009) 123505, [[arXiv:0802.2922](#)].
- [10] O. Adriani *et al.*, *A new measurement of the antiproton-to-proton flux ratio up to 100 GeV in the cosmic radiation*, *Phys. Rev. Lett.* **102** (2009) 051101, [[arXiv:0810.4994](#)].
- [11] M. Pospelov, A. Ritz, and M. B. Voloshin, *Secluded WIMP Dark Matter*, *Phys. Lett.* **B662** (2008) 53–61, [[arXiv:0711.4866](#)].
- [12] M. Pospelov and A. Ritz, *Astrophysical Signatures of Secluded Dark Matter*, *Phys. Lett.* **B671** (2009) 391–397, [[arXiv:0810.1502](#)].
- [13] A. E. Nelson and C. Spitzer, *Slightly Non-Minimal Dark Matter in PAMELA and ATIC*, [arXiv:0810.5167](#).
- [14] I. Cholis, D. P. Finkbeiner, L. Goodenough, and N. Weiner, *The PAMELA Positron Excess from Annihilations into a Light Boson*, [arXiv:0810.5344](#).
- [15] Y. Nomura and J. Thaler, *Dark Matter through the Axion Portal*, *Phys. Rev.* **D79** (2009) 075008, [[arXiv:0810.5397](#)].
- [16] D. Tucker-Smith and N. Weiner, *Inelastic dark matter*, *Phys. Rev.* **D64** (2001) 043502, [[hep-ph/0101138](#)].
- [17] S. Chang, G. D. Kribs, D. Tucker-Smith, and N. Weiner, *Inelastic Dark Matter in Light of DAMA/LIBRA*, *Phys. Rev.* **D79** (2009) 043513, [[arXiv:0807.2250](#)].
- [18] A. Katz and R. Sundrum, *Breaking the Dark Force*, *JHEP* **06** (2009) 003, [[arXiv:0902.3271](#)].

- [19] G. Duda, G. Gelmini, and P. Gondolo, *Detection of a subdominant density component of cold dark matter*, *Phys. Lett.* **B529** (2002) 187–192, [[hep-ph/0102200](#)].
- [20] G. Duda, G. Gelmini, P. Gondolo, J. Edsjo, and J. Silk, *Indirect detection of a subdominant density component of cold dark matter*, *Phys. Rev.* **D67** (2003) 023505, [[hep-ph/0209266](#)].
- [21] K. M. Zurek, *Multi-Component Dark Matter*, *Phys. Rev.* **D79** (2009) 115002, [[arXiv:0811.4429](#)].
- [22] D. P. Finkbeiner, N. Padmanabhan, and N. Weiner, *CMB and 21-cm Signals for Dark Matter with a Long-Lived Excited State*, *Phys. Rev.* **D78** (2008) 063530, [[arXiv:0805.3531](#)].
- [23] N. Arkani-Hamed and N. Weiner, *LHC Signals for a SuperUnified Theory of Dark Matter*, *JHEP* **12** (2008) 104, [[arXiv:0810.0714](#)].
- [24] E. W. Kolb and M. S. Turner, *The early universe*. Frontiers in Physics, Reading, MA: Addison-Wesley, 1990.
- [25] A. Sommerfeld, *Über die Beugung und Bremsung der Elektronen*, *Annalen der Physik* **403** (1931) 257–330.
- [26] J. Hisano, S. Matsumoto, M. M. Nojiri, and O. Saito, *Non-perturbative effect on dark matter annihilation and gamma ray signature from galactic center*, *Phys. Rev.* **D71** (2005) 063528, [[hep-ph/0412403](#)].
- [27] M. Cirelli, R. Franceschini, and A. Strumia, *Minimal Dark Matter predictions for galactic positrons, anti-protons, photons*, *Nucl. Phys.* **B800** (2008) 204–220, [[arXiv:0802.3378](#)].
- [28] J. March-Russell, S. M. West, D. Cumberbatch, and D. Hooper, *Heavy Dark Matter Through the Higgs Portal*, *JHEP* **07** (2008) 058, [[arXiv:0801.3440](#)].
- [29] B. Holdom, *Two $U(1)$'s and Epsilon Charge Shifts*, *Phys. Lett.* **B166** (1986) 196.
- [30] M. Pospelov and A. Ritz, *The galactic 511-keV line from electroweak scale WIMPs*, *Phys. Lett.* **B651** (2007) 208–215, [[hep-ph/0703128](#)].
- [31] F. Chen, J. M. Cline, and A. R. Frey, *Nonabelian dark matter: models and constraints*, *Phys. Rev.* **D80** (2009) 083516, [[arXiv:0907.4746](#)].
- [32] D. P. Finkbeiner, T. R. Slatyer, N. Weiner, and I. Yavin, *PAMELA, DAMA, INTEGRAL and Signatures of Metastable Excited WIMPs*, *JCAP* **0909** (2009) 037, [[arXiv:0903.1037](#)].
- [33] F. Governato, *Private communication*, 2009.
- [34] E. Romano-Diaz, I. Shlosman, Y. Hoffman, and C. Heller, *Erasing Dark Matter Cusps in Cosmological Galactic Halos with Baryons*, [arXiv:0808.0195](#).
- [35] E. Romano-Diaz, I. Shlosman, C. Heller, and Y. Hoffman, *Dissecting Galaxy Formation: I. Comparison Between Pure Dark Matter and Baryonic Models*, *Astrophys. J.* **702** (2009) 1250–1267, [[arXiv:0901.1317](#)].
- [36] M. G. Abadi, J. F. Navarro, M. Fardal, A. Babul, and M. Steinmetz, *Galaxy-Induced Transformation of Dark Matter Halos*, [arXiv:0902.2477](#).
- [37] S. E. Pedrosa, P. B. Tissera, and C. Scannapieco, *The joint evolution of baryons and dark matter haloes*, [arXiv:0910.4380](#).

- [38] F. Chen, J. M. Cline, A. Fradette, A. R. Frey, and C. Rabideau, *Exciting dark matter in the galactic center*, [arXiv:0911.2222](#).
- [39] R. Morris *et al.*, *In progress*, .
- [40] J. March-Russell, C. McCabe, and M. McCullough, *Inelastic Dark Matter, Non-Standard Halos and the DAMA/LIBRA Results*, *JHEP* **05** (2009) 071, [[arXiv:0812.1931](#)].
- [41] Y. Cui, D. E. Morrissey, D. Poland, and L. Randall, *Candidates for Inelastic Dark Matter*, *JHEP* **05** (2009) 076, [[arXiv:0901.0557](#)].
- [42] D. B. Cline, W. Ooi, and H. Wang, *Constraints on Inelastic Dark Matter Signal using ZEPLIN- II Results*, [arXiv:0906.4119](#).
- [43] X. Collaboration, *Constraints on inelastic dark matter from XENON10*, [arXiv:0910.3698](#).
- [44] M. Kuhlen and N. Weiner, *In progress*, .
- [45] D. E. Morrissey, D. Poland, and K. M. Zurek, *Abelian Hidden Sectors at a GeV*, *JHEP* **07** (2009) 050, [[arXiv:0904.2567](#)].
- [46] M. Baumgart, C. Cheung, J. T. Ruderman, L.-T. Wang, and I. Yavin, *Non-Abelian Dark Sectors and Their Collider Signatures*, *JHEP* **04** (2009) 014, [[arXiv:0901.0283](#)].
- [47] C. Cheung, J. T. Ruderman, L.-T. Wang, and I. Yavin, *Kinetic Mixing as the Origin of Light Dark Scales*, *Phys. Rev.* **D80** (2009) 035008, [[arXiv:0902.3246](#)].
- [48] D. P. Finkbeiner, T. R. Slatyer, and N. Weiner, *Nuclear scattering of dark matter coupled to a new light scalar*, *Phys. Rev.* **D78** (2008) 116006, [[arXiv:0810.0722](#)].
- [49] C. Boehm and P. Fayet, *Scalar dark matter candidates*, *Nucl. Phys.* **B683** (2004) 219–263, [[hep-ph/0305261](#)].
- [50] J. T. Ruderman and T. Volansky, *Searching for Smoking Gun Signatures of Decaying Dark Matter*, [arXiv:0907.4373](#).
- [51] J. T. Ruderman and T. Volansky, *Decaying into the Hidden Sector*, [arXiv:0908.1570](#).
- [52] M. Pospelov, *Secluded $U(1)$ below the weak scale*, *Phys. Rev.* **D80** (2009) 095002, [[arXiv:0811.1030](#)].
- [53] B. Batell, M. Pospelov, and A. Ritz, *Probing a Secluded $U(1)$ at B-factories*, *Phys. Rev.* **D79** (2009) 115008, [[arXiv:0903.0363](#)].
- [54] M. Reece and L.-T. Wang, *Searching for the light dark gauge boson in GeV-scale experiments*, *JHEP* **07** (2009) 051, [[arXiv:0904.1743](#)].
- [55] P.-f. Yin, J. Liu, and S.-h. Zhu, *Detecting light leptophilic gauge boson at BESIII detector*, *Phys. Lett.* **B679** (2009) 362–368, [[arXiv:0904.4644](#)].
- [56] C. Cheung, J. T. Ruderman, L.-T. Wang, and I. Yavin, *Lepton Jets in (Supersymmetric) Electroweak Processes*, [arXiv:0909.0290](#).
- [57] B. Batell, M. Pospelov, and A. Ritz, *Multi-lepton Signatures of a Hidden Sector in Rare B Decays*, [arXiv:0911.4938](#).

- [58] J. Liu, P.-f. Yin, and S.-h. Zhu, *Prospects for Detecting Neutrino Signals from Annihilating/Decaying Dark Matter to Account for the PAMELA and ATIC results*, *Phys. Rev. D* **79** (2009) 063522, [[arXiv:0812.0964](#)].
- [59] B. Batell, M. Pospelov, A. Ritz, and Y. Shang, *Solar Gamma Rays Powered by Secluded Dark Matter*, [arXiv:0910.1567](#).
- [60] P. Schuster, N. Toro, and I. Yavin, *Terrestrial and Solar Limits on Long-Lived Particles in a Dark Sector*, [arXiv:0910.1602](#).
- [61] P. Schuster, N. Toro, N. Weiner, and I. Yavin, *High Energy Electron Signals from Dark Matter Annihilation in the Sun*, [arXiv:0910.1839](#).
- [62] P. Meade, S. Nussinov, M. Papucci, and T. Volansky, *Searches for Long Lived Neutral Particles*, [arXiv:0910.4160](#).
- [63] P.-f. Yin and S.-h. Zhu, *Detecting light long-lived particle produced by cosmic ray*, [arXiv:0911.3338](#).
- [64] **AMS** Collaboration, M. Aguilar *et al.*, *The Alpha Magnetic Spectrometer (AMS) on the International Space Station. I: Results from the test flight on the space shuttle*, *Phys. Rept.* **366** (2002) 331–405.
- [65] N. Padmanabhan and D. P. Finkbeiner, *Detecting Dark Matter Annihilation with CMB Polarization : Signatures and Experimental Prospects*, *Phys. Rev. D* **72** (2005) 023508, [[astro-ph/0503486](#)].
- [66] S. Galli, F. Iocco, G. Bertone, and A. Melchiorri, *CMB constraints on Dark Matter models with large annihilation cross-section*, *Phys. Rev. D* **80** (2009) 023505, [[arXiv:0905.0003](#)].
- [67] T. R. Slatyer, N. Padmanabhan, and D. P. Finkbeiner, *CMB Constraints on WIMP Annihilation: Energy Absorption During the Recombination Epoch*, *Phys. Rev. D* **80** (2009) 043526, [[arXiv:0906.1197](#)].
- [68] S. Profumo, *Dissecting Pamela (and ATIC) with Occam’s Razor: existing, well-known Pulsars naturally account for the ‘anomalous’ Cosmic-Ray Electron and Positron Data*, [arXiv:0812.4457](#).
- [69] D. Malyshev, I. Cholis, and J. Gelfand, *Pulsars versus Dark Matter Interpretation of ATIC/PAMELA*, *Phys. Rev. D* **80** (2009) 063005, [[arXiv:0903.1310](#)].
- [70] N. Kawanaka, K. Ioka, and M. M. Nojiri, *Cosmic-Ray Electron Excess from Pulsars is Spiky or Smooth?: Continuous and Multiple Electron/Positron injections*, [arXiv:0903.3782](#).
- [71] P. H. Frampton and P. Q. Hung, *Positron Excess, Luminous-Dark Matter Unification and Family Structure*, *Phys. Lett. B* **675** (2009) 411–414, [[arXiv:0903.0358](#)].
- [72] J. Mardon, Y. Nomura, D. Stolarski, and J. Thaler, *Dark Matter Signals from Cascade Annihilations*, *JCAP* **0905** (2009) 016, [[arXiv:0901.2926](#)].
- [73] I. Cholis, L. Goodenough, and N. Weiner, *In preparation*, .
- [74] I. Cholis, G. Dobler, D. P. Finkbeiner, L. Goodenough, and N. Weiner, *The Case for a 700+ GeV WIMP: Cosmic Ray Spectra from ATIC and PAMELA*, [arXiv:0811.3641](#).

- [75] J. Zhang *et al.*, *Discriminating different scenarios to account for the cosmic $e + /-$ excess by synchrotron and inverse Compton radiation*, *Phys. Rev.* **D80** (2009) 023007, [[arXiv:0812.0522](#)].
- [76] E. Borriello, A. Cuoco, and G. Miele, *Secondary radiation from the Pamela/ATIC excess and relevance for Fermi*, *Astrophys. J.* **699** (2009) L59–L63, [[arXiv:0903.1852](#)].
- [77] M. Cirelli and P. Panci, *Inverse Compton constraints on the Dark Matter $e+e-$ excesses*, *Nucl. Phys.* **B821** (2009) 399–416, [[arXiv:0904.3830](#)].
- [78] M. Regis and P. Ullio, *Testing the Dark Matter Interpretation of the PAMELA Excess through Measurements of the Galactic Diffuse Emission*, *Phys. Rev.* **D80** (2009) 043525, [[arXiv:0904.4645](#)].
- [79] A. V. Belikov and D. Hooper, *The Contribution Of Inverse Compton Scattering To The Diffuse Extragalactic Gamma-Ray Background From Annihilating Dark Matter*, [arXiv:0906.2251](#).
- [80] P. Meade, M. Papucci, A. Strumia, and T. Volansky, *Dark Matter Interpretations of the Electron/Positron Excesses after FERMI*, [arXiv:0905.0480](#).
- [81] G. Dobler, D. P. Finkbeiner, I. Cholis, T. R. Slatyer, and N. Weiner, *The Fermi Haze: A Gamma-Ray Counterpart to the Microwave Haze*, [arXiv:0910.4583](#).
- [82] F.-Y. Cyr-Racine, S. Profumo, and K. Sigurdson, *Protohalo Constraints to the Resonant Annihilation of Dark Matter*, *Phys. Rev.* **D80** (2009) 081302, [[arXiv:0904.3933](#)].
- [83] S. Profumo and T. E. Jeltema, *Extragalactic Inverse Compton Light from Dark Matter Annihilation and the Pamela Positron Excess*, *JCAP* **0907** (2009) 020, [[arXiv:0906.0001](#)].
- [84] T. R. Slatyer, *The Sommerfeld enhancement for dark matter with an excited state*, [arXiv:0910.5713](#).
- [85] L. Bergstrom, T. Bringmann, M. Eriksson, and M. Gustafsson, *Gamma rays from Kaluza-Klein dark matter*, *Phys. Rev. Lett.* **94** (2005) 131301, [[astro-ph/0410359](#)].
- [86] A. Birkedal, K. T. Matchev, M. Perelstein, and A. Spray, *Robust gamma ray signature of WIMP dark matter*, [hep-ph/0507194](#).
- [87] G. D. Mack, T. D. Jacques, J. F. Beacom, N. F. Bell, and H. Yuksel, *Conservative Constraints on Dark Matter Annihilation into Gamma Rays*, *Phys. Rev.* **D78** (2008) 063542, [[arXiv:0803.0157](#)].
- [88] M. Cirelli, M. Kadastik, M. Raidal, and A. Strumia, *Model-independent implications of the $e+$, $e-$, anti-proton cosmic ray spectra on properties of Dark Matter*, *Nucl. Phys.* **B813** (2009) 1–21, [[arXiv:0809.2409](#)].
- [89] L. Bergstrom, G. Bertone, T. Bringmann, J. Edsjo, and M. Taoso, *Gamma-ray and Radio Constraints of High Positron Rate Dark Matter Models Annihilating into New Light Particles*, *Phys. Rev.* **D79** (2009) 081303, [[arXiv:0812.3895](#)].
- [90] P. Meade, M. Papucci, and T. Volansky, *Dark Matter Sees The Light*, [arXiv:0901.2925](#).
- [91] J.-F. Fortin, J. Shelton, S. Thomas, and Y. Zhao, *Gamma Ray Spectra from Dark Matter Annihilation and Decay*, [arXiv:0908.2258](#).

- [92] D. P. Finkbeiner, *WMAP microwave emission interpreted as dark matter annihilation in the inner Galaxy*, [astro-ph/0409027](#).
- [93] D. Hooper, D. P. Finkbeiner, and G. Dobler, *Evidence Of Dark Matter Annihilations In The WMAP Haze*, *Phys. Rev.* **D76** (2007) 083012, [[arXiv:0705.3655](#)].
- [94] G. Dobler and D. P. Finkbeiner, *Extended Anomalous Foreground Emission in the WMAP 3-Year Data*, *Astrophys. J.* **680** (2008) 1222–1234, [[arXiv:0712.1038](#)].
- [95] M. S. Longair, *High Energy Astrophysics, Volume 2, pp. 239-252*. Cambridge University Press, 2002.
- [96] **WMAP** Collaboration, C. L. Bennett *et al.*, *First Year Wilkinson Microwave Anisotropy Probe (WMAP) Observations: Preliminary Maps and Basic Results*, *Astrophys. J. Suppl.* **148** (2003) 1, [[astro-ph/0302207](#)].
- [97] N. Mandolesi, M. Bersanelli, C. Burigana, and F. Villa, *The Planck Low Frequency Instrument*, *AIP Conf. Proc.* **616** (2002) 193–201, [[astro-ph/9904135](#)].
- [98] A. Mennella *et al.*, *The Low Frequency Instrument in the ESA Planck mission*, *AIP Conf. Proc.* **703** (2004) 401–404, [[astro-ph/0310058](#)].
- [99] J.-M. Lamarre *et al.*, *The Planck High Frequency Instrument, a 3rd generation CMB experiment, and a full sky submillimeter survey*, [astro-ph/0308075](#).
- [100] **Planck** Collaboration, *Planck: The scientific programme*, [astro-ph/0604069](#).
- [101] D. P. Finkbeiner, *Microwave ISM Emission Observed by WMAP*, *Astrophys. J.* **614** (2004) 186–193, [[astro-ph/0311547](#)].
- [102] R. Jansson, G. R. Farrar, A. H. Waelkens, and T. A. Ensslin, *Constraining models of the large scale Galactic magnetic field with WMAP5 polarization data and extragalactic Rotation Measure sources*, *JCAP* **0907** (2009) 021, [[arXiv:0905.2228](#)].
- [103] X. H. Sun, W. Reich, A. Waelkens, and T. Ensslin, *Radio observational constraints on Galactic 3D-emission models*, [arXiv:0711.1572](#).
- [104] J. C. Brown *et al.*, *Rotation Measures of Extragalactic Sources Behind the Southern Galactic Plane: New Insights into the Large- Scale Magnetic Field of the Inner Milky Way*, *Astrophys. J.* **663** (2007) 258–266, [[arXiv:0704.0458](#)].
- [105] Y. Sofue and M. Fujimoto, *A bisymmetric spiral magnetic field and the spiral arms in our Galaxy*, *ApJ* **265** (Feb., 1983) 722–729.
- [106] J. L. Han and G. J. Qiao, *The magnetic field in the disk of our Galaxy*, *Astron. Astrophys.* **288** (Aug., 1994) 759–772.
- [107] R. Beck, *Galactic and extragalactic magnetic fields*, *Space Sci. Rev.* **99** (2001) 243–260, [[astro-ph/0012402](#)].
- [108] J. Han, *Magnetic fields in our Galaxy: How much do we know? (II) Halo fields and the global field structure*, [astro-ph/0110319](#).
- [109] P. G. Tinyakov and I. I. Tkachev, *Tracing protons through the galactic magnetic field: A clue for charge composition of ultrahigh-energy cosmic rays*, *Astropart. Phys.* **18** (2002) 165–172, [[astro-ph/0111305](#)].

- [110] C. G. T. Haslam, C. J. Salter, H. Stoffel, and W. E. Wilson, *A 408 MHz all-sky continuum survey. II - The atlas of contour maps*, *Astron. Astrophys. Supp.* **47** (Jan., 1982) 1–+.
- [111] D. P. F. L. G. T. R. S. Gregory Dobler, Ilias Cholis and N. Weiner., *In preparation*, .
- [112] **DAMA** Collaboration, R. Bernabei *et al.*, *First results from DAMA/LIBRA and the combined results with DAMA/NaI*, *Eur. Phys. J.* **C56** (2008) 333–355, [[arXiv:0804.2741](#)].
- [113] T. Kobayashi, Y. Komori, K. Yoshida, and J. Nishimura, *The most likely sources of high energy cosmic-ray electrons in supernova remnants*, *Astrophys. J.* **601** (2004) 340–351, [[astro-ph/0308470](#)].
- [114] A. Boulares, *The nature of the cosmic-ray electron spectrum, and supernova remnant contributions*, *ApJ* **342** (July, 1989) 807–813.
- [115] M. Pohl and J. A. Esposito, *Electron acceleration in SNR and diffuse gamma-rays above 1-GeV*, [astro-ph/9806160](#).
- [116] I. Büsching, M. Pohl, and R. Schlickeiser, *Excess GeV radiation and cosmic ray origin*, in *Gamma 2001: Gamma-Ray Astrophysics* (S. Ritz, N. Gehrels, & C. R. Shrader, ed.), vol. 587 of *American Institute of Physics Conference Series*, pp. 469–473, Oct., 2001.
- [117] A. W. Strong, I. V. Moskalenko, and O. Reimer, *Diffuse Galactic continuum gamma rays. A model compatible with EGRET data and cosmic-ray measurements*, *Astrophys. J.* **613** (2004) 962–976, [[astro-ph/0406254](#)].
- [118] V. S. Ptuskin, F. C. Jones, E. S. Seo, and R. Sina, *Effect of random nature of cosmic ray sources Supernova remnants on cosmic ray intensity fluctuations, anisotropy, and electron energy spectrum*, *Advances in Space Research* **37** (2006) 1909–1912.
- [119] J. H. Taylor and D. R. Stinebring, *Recent progress in the understanding of pulsars*, *ARAAS* **24** (1986) 285–327.
- [120] A. M. Atoyan, F. A. Aharonian, and H. J. Völk, *Electrons and positrons in the galactic cosmic rays*, *PRD* **52** (Sept., 1995) 3265–3275.
- [121] D. Hooper, P. Blasi, and P. D. Serpico, *Pulsars as the Sources of High Energy Cosmic Ray Positrons*, *JCAP* **0901** (2009) 025, [[arXiv:0810.1527](#)].
- [122] H. Yuksel, M. D. Kistler, and T. Stanev, *TeV Gamma Rays from Geminga and the Origin of the GeV Positron Excess*, *Phys. Rev. Lett.* **103** (2009) 051101, [[arXiv:0810.2784](#)].
- [123] D. N. Spergel and P. J. Steinhardt, *Observational evidence for self-interacting cold dark matter*, *Phys. Rev. Lett.* **84** (2000) 3760–3763, [[astro-ph/9909386](#)].
- [124] L. Ackerman, M. R. Buckley, S. M. Carroll, and M. Kamionkowski, *Dark Matter and Dark Radiation*, *Phys. Rev.* **D79** (2009) 023519, [[arXiv:0810.5126](#)].
- [125] P. J. Fox and M. R. Buckley, *Dark Matter Self-Interactions and Light Force Carriers*, [arXiv:0911.3898](#).
- [126] J. L. Feng, M. Kaplinghat, and H.-B. Yu, *Halo Shape and Relic Density Exclusions of Sommerfeld- Enhanced Dark Matter Explanations of Cosmic Ray Excesses*, [arXiv:0911.0422](#).
- [127] D. Merritt, J. F. Navarro, A. Ludlow, and A. Jenkins, *A Universal Density Profile for Dark and Luminous Matter?*, *Astrophys. J.* **624** (2005) L85–L88, [[astro-ph/0502515](#)].

- [128] J. Holmberg and C. Flynn, *The local density of matter mapped by Hipparcos*, *Mon. Not. Roy. Astron. Soc.* **313** (2000) 209–216, [[astro-ph/9812404](#)].
- [129] M. Creze, E. Chereul, O. Bienayme, and C. P. C. d. D. a. d. S. I. Basel, *The distribution of nearby stars in phase space mapped by Hipparcos: I. The potential well and local dynamical mass*, [astro-ph/9709022](#).
- [130] J. Holmberg and C. Flynn, *The local surface density of disc matter mapped by Hipparcos*, *Mon. Not. Roy. Astron. Soc.* **352** (2004) 440, [[astro-ph/0405155](#)].
- [131] V. I. Korchagin, T. M. Girard, T. V. Borkova, D. I. Dinescu, and W. F. van Altena, *Local Surface Density of the Galactic Disk from a 3-D Stellar Velocity Sample*, [astro-ph/0308276](#).
- [132] R. Catena and P. Ullio, *A novel determination of the local dark matter density*, [arXiv:0907.0018](#).
- [133] D. Hooper, A. Stebbins, and K. M. Zurek, *Excesses in cosmic ray positron and electron spectra from a nearby clump of neutralino dark matter*, *Phys. Rev.* **D79** (2009) 103513, [[arXiv:0812.3202](#)].
- [134] M. Kuhlen and D. Malyshev, *Model in-dependence of electron and positron flux from Dark Matter*, *Phys. Rev.* **D79** (2009) 123517, [[arXiv:0904.3378](#)].
- [135] A. W. Strong, I. V. Moskalenko, and V. S. Ptuskin, *Cosmic-ray propagation and interactions in the Galaxy*, *Ann. Rev. Nucl. Part. Sci.* **57** (2007) 285–327, [[astro-ph/0701517](#)].
- [136] T. A. Porter and A. W. Strong, *A new estimate of the Galactic interstellar radiation field between 0.1 microns and 1000 microns*, [astro-ph/0507119](#).
- [137] R. Schlickeiser, *Cosmic Ray Astrophysics*, pp. 116-127. Springer, 2002.
- [138] **WMAP** Collaboration, G. Hinshaw *et al.*, *Five-Year Wilkinson Microwave Anisotropy Probe (WMAP) Observations: Data Processing, Sky Maps, & Basic Results*, *Astrophys. J. Suppl.* **180** (2009) 225–245, [[arXiv:0803.0732](#)].